ΠΑΡΑΡΤΗΜΑ Ι

Επιστημονικές Εργασίες

Δελτίο της Ελληνικής Γεωλογικής Εταιρίας, Τομ. XXXIV/1, 303-309, 2001
Πρακτικά 9ου Διεθνούς Συνεδρίου, Αθήνα, Σεπτέμβριος 2001

Bulletin of the Geological Society of Greece, Vol. XXXIV/1, 303-309, 2001
Proceedings of the 9th International Congress, Athens, September 2001

A STUDY OF THE ACTIVE TECTONICS AND DEFORMATION IN THE MYGDONIA BASIN (N.GREECE) USING SEISMOLOGICAL AND NEOTECTONIC DATA

PAPAZACHOS, C.B.[1], VAMVAKARIS, D.A.[1], VARGEMEZIS, G.N.[1] AND AIDONA, E.V.[1]

ABSTRACT

In the present work we study the active tectonics setting and related deformation scheme in the Mygdonia basin, on the basis of the joint interpretation of seismological and neotectonic data. For this reason, the stress field derived from fault plane solutions of small-magnitude events from a local seismological experiment, as well as neotectonic observations are studied in order to determine its spatial distribution. The results show an almost identical spatial variation of the stress field determined from the two independent data sets, which also exhibits a very good correlation with the geomorphological changes in the Mygdonia basin. Moreover, the average stress field is almost identical to the corresponding stress pattern determined from the 3 largest events in the study area for which reliable fault plane solutions are available. Using the combined stress pattern and the corresponding moment-rate tensors derived from both data sets, the active crustal deformation is studied for the most active sections of the Mygdonia basin system. The results show a N-S extension at an average rate of 3mm/yr for the central part of the Mygdonia system, in very good agreement with the available geodetic results.

KEYWORDS: Stress field, active deformation, strain tensor, Mygdonia basin

THE MYGDONIA BASIN AREA

The Mygdonia basin is one of the most active seismogenic regions in the back-arc Aegean area. The basin is located at the centre of the Servomacedonian massif, which is surrounded by a series of basins/troughs, namely the Axios and Strymon basins and the North Aegean Trough (fig.1). The seismicity of the Servomacedonian massif which extends from the Yugoslavia-Bulgaria border up to the North Aegean Trough is the highest in N. Greece with events up to M_W=7.6. A large portion of this seismic activity is located in the Mygdonia basin and its continuation towards the Ierissos bay area. The basin has a characteristic S-shape (see fig. 1) with its edges trending in a NW-SE direction, while the central part is approximately E-W oriented. This central section is the most seismically active and has received a lot of scientific attention, since the occurrence of the M_W=6.5

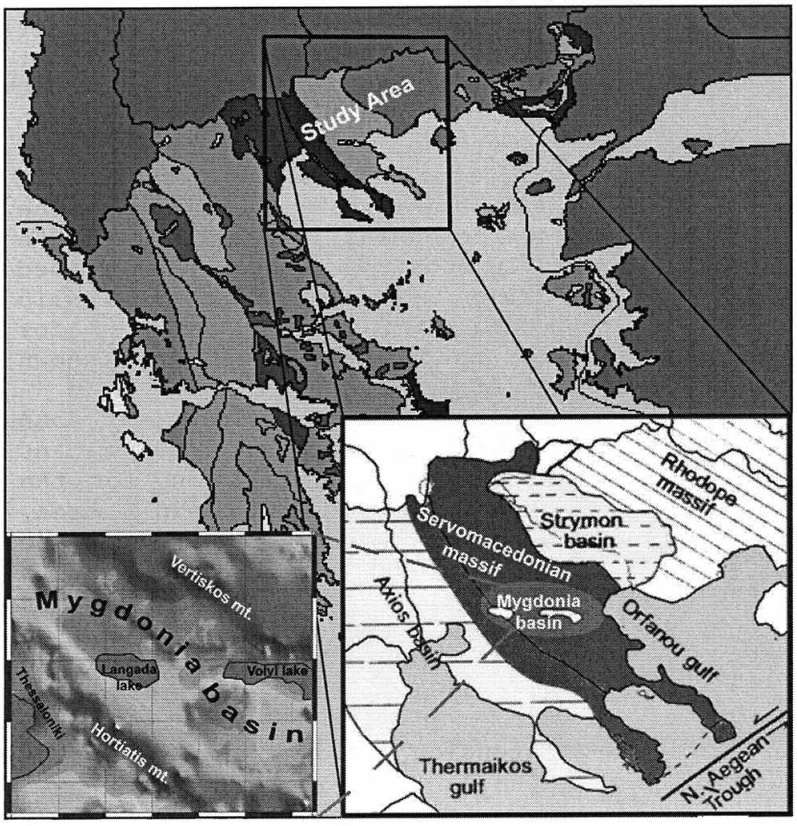

Fig. 1. Map of the main geological zones of Greece. The inset figures show the detailed ~~geomorphological features~~ of the Mygdonia basin.

[1] Dept. of Geophysics, School of Geology, Aristotle University of Thessaloniki, PO Box 352-1, Thessaloniki, GR-54006, GREECE

mainshock of June 20, 1978, which was the first major event with significance impact on a modern urban centre like the city of Thessaloniki (Papazachos et al., 1979; Pavlides and Kilias, 1987; Pavlides et al., 1988; Hatzidimitriou et al., 1991).

DATA USED

The data used consist of three different datasets. The first data set corresponds to the fault plane solutions determined from the analysis of earthquakes recorded by a local network which operated in the Mygdonia area in the springs of 1984 and 1985 (Christodoulou, 1986; Hatzfeld et al., 1987). Additional fault plane solutions for the Asvestochori area were used from the work of Papazachos et al. (2000). All these fault plane solutions correspond to small magnitude events ($M_W \leq 3.1$) and their distribution is presented in figure 2. In the same figure, the fault plane solutions of the 3 mainshocks ($M_W > 5.5$) that have occurred in the area for which reliable fault plane solutions were available are also shown. These mainshocks (1978/5/23, M_W=5.8, Volvi preshock; 1978/6/20, M_W=6.5, Volvi mainshock; 1995/5/4, M_W=5.8, Arnaia mainshock) represent the second dataset used. The last dataset corresponds to the neotectonic faults and related information reported in the neotectonic maps of "Langadas" and "Thessaloniki" (Mountrakis et al., 1997). The corresponding fault plane solutions, which were determined using the fault plane and slip vector information reported for the neotectonic faults are shown in figure 3.

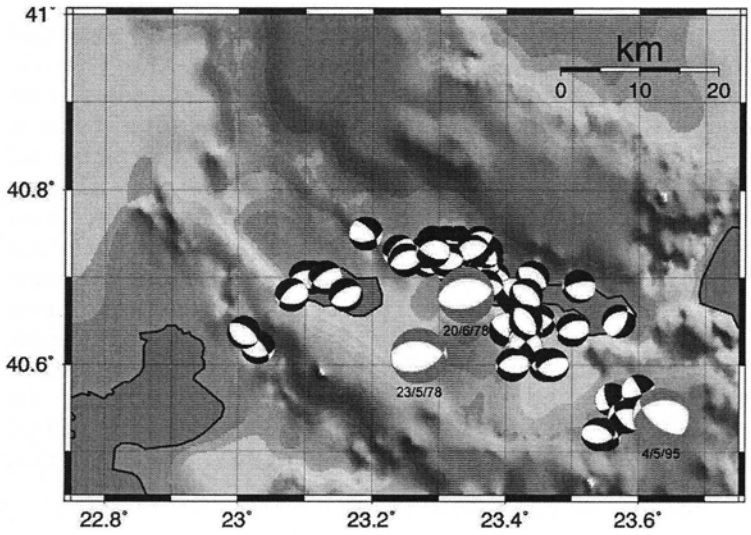

Fig. 2. Fault plane solutions determined for 63 small earthquakes recorded in the spring of 1984 and 1985 (black solutions). The solutions of the 3 main earthquakes ($M_W > 5.5$) are also shown (grey solutions).

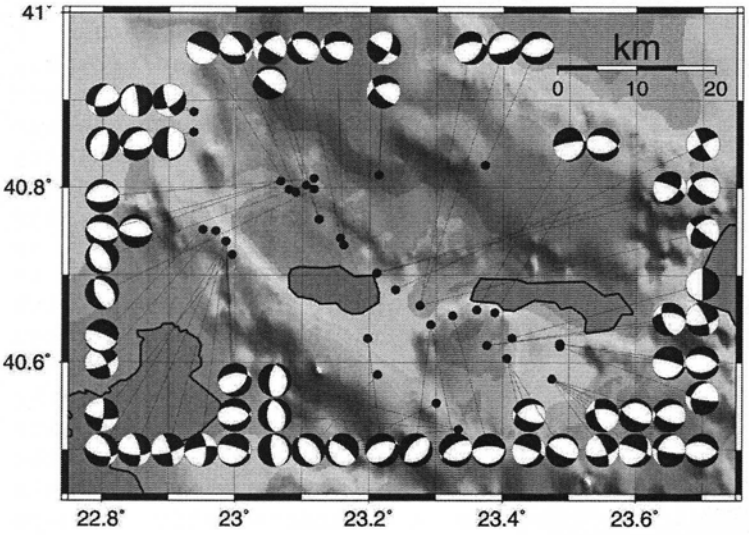

Fig. 3. Fault plane solutions corresponding to the neotectonic faults of the broader Mygdonia basin (see text for explanations).

Both the seismological and neotectonic data show a dominant normal type of faulting for the whole Mygdonia basin area. Although the small-magnitude events and small-scale faults exhibit a variety of fault azimuths, most events, as well as the 3 largest mainshocks show an average E-W fault direction, in agreement with the general basin lineation, which corresponds to an average N-S extension field.

APPLIED METHOD

In order to study the active crustal deformation we applied the method of Papazachos and Kiratzi (1992). The method is based on the originally proposed results of Kostrov (1974) and Jackson and McKenzie (1988) and relies on the use of all complete seismicity data for the estimation of the size of the

deformation and all the available fault plane solutions, which do not need to be complete for the examined time period. Using this approach, the problem of complete fault plane solution data can be overcome using information derived from other sources. Such sources are the historical seismicity for the estimation of the deformation rate or field active-faults observations for the determination of the deformation pattern.

For the estimation of the strain rate tensor, $\dot{\varepsilon}_{ij}$, and the velocity tensor, U_{ij}, the following equations are used (Papazachos and Kiratzi, 1992):

$$\dot{\varepsilon}_{ij} = \frac{1}{2\mu V}\,\dot{M}_o \cdot \bar{F}_{ij} \quad i,j = 1,2,3 \qquad U_{ii} = \frac{1}{2\mu l_k l_j}\,\dot{M}_o \cdot \bar{F}_{ii} \quad i \neq k,\ k \neq j,\ j \neq i,\ i = 1,2,3 \qquad (1)$$

$$U_{12} = \frac{1}{\mu l_1 l_2}\,\dot{M}_o \cdot \bar{F}_{12} \qquad U_{i3} = \frac{1}{\mu l_1 l_3}\,\dot{M}_o \cdot \bar{F}_{i3} \quad i = 1,2$$

where l_1, l_2, l_3, are the dimensions of the deforming zone, μ is the shear modulus (usually taken 3.10^{11}dyn/cm^2) and, $\dot{M}_o$, is the released moment rate which is defined by the seismicity level of the area, and is determined using the relation of Molnar (1979):

$$\dot{M}_0 = \frac{A}{1-B} \bullet M_{0,\max}^{1-B} \qquad (2)$$

where $M_{0,max}$ corresponds to the seismic moment of the maximum-magnitude event in the deforming zone. Constants A and B can be determined using the Gutenberg-Richter parameters of the zone and the constants of the seismic moment-magnitude relation using, appropriate formulas. $\bar{F}$ is the average "focal mechanism" tensor, which represents the deformation pattern of the area and is the average of the individual F^n tensors which correspond to each fault plane solution and are a function of the corresponding strike, ζ, dip, δ, and rake, λ (Aki and Richards, 1980).

As can be seen from equations (1), the estimation of the strain and velocity tensors is decomposed in the estimation of the moment-rate and the representative focal mechanism tensor. For this reason the estimation of the active deformation can be performed in two steps:

a) Areas with similar tectonic characteristics can be grouped in order to define a reliable average "focal mechanism" tensor, using all fault plane data.

b) The moment-rate is estimated using the complete

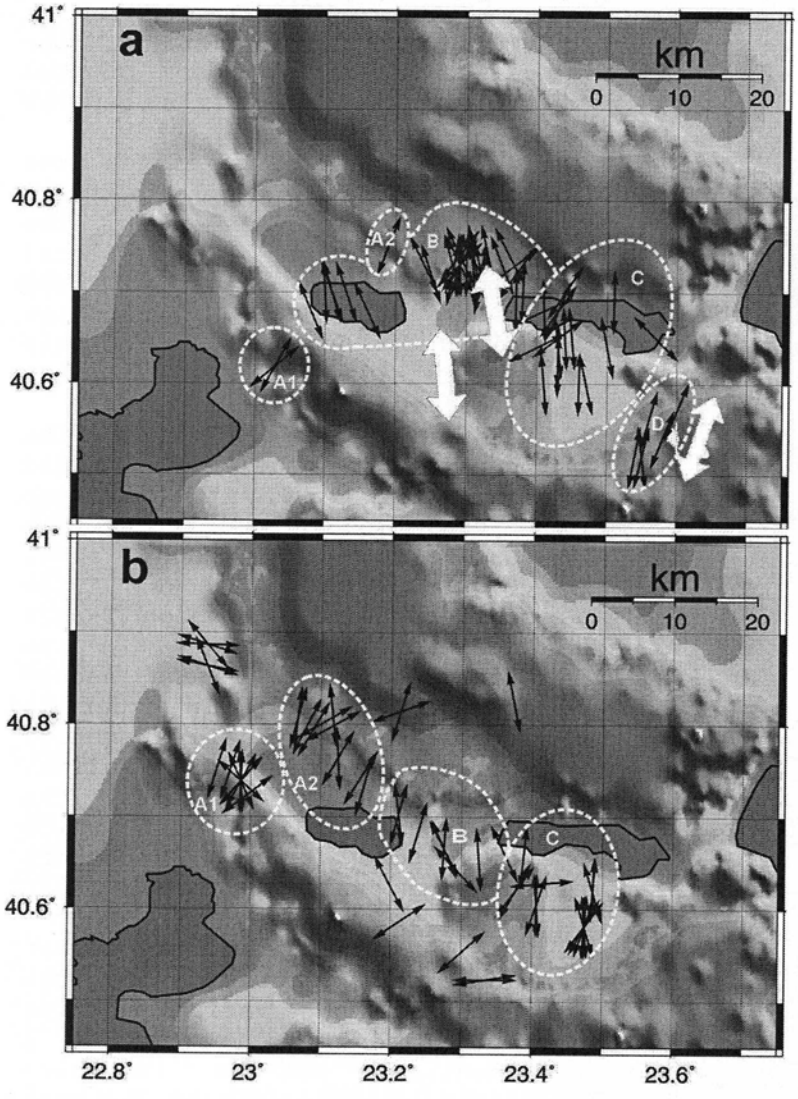

Fig. 4. a) Extensional T-axes for the 63 small earthquakes (black arrows) and the 3 main events with M>5.5 (white arrows), grouped in zones with similar tectonic characteristics. a) Same as (a) for the neotectonic data.

instrumental and historical seismicity through the Gutenberg-Richter relation and equation (2).

IDENTIFICATION OF ZONES OF SIMILAR FAULTING

In order to define zones of similar tectonic setting, the spatial distribution of the stress axes was studied, as these are defined by the corresponding fault plane solutions. Since the study area is dominated by extension, the zone identification was mainly based on the similarity of the T-axes. Figure 4a shows the T-axis distribution for the earthquake data, while 4b shows the corresponding distribution for the neotectonic data. In general 4 main zones are recognized:

a) Zone A. This zone corresponds to the north (A1) and south (A2) NW-SE trending borders of the western part of the Mygdonia basin system. In general a NE-SE tension field dominates this basin borders, although limited data are available from the seismological experiments.

b) Zone B. This zones includes the central main part of the Mygdonia basin and includes the Langada lake, the central basin parts between the Langada and Volvi lakes, as well as the westernmost section of the Volvi lake. The tension axis of both seismological and neotectonic data shows a N-S to NNE-SSE direction, in agreement with the T-axis of the 1978 Volvi events (1978/5/23, M_W=5.8 and 1978/6/20, M_W=6.5), which are also shown with large white arrows.

c) Zone C. The zone corresponds to the largest part of the Volvi lake, as well as the section of the Mygdonia basin south of the Volvi lake, showing a general N-S extension field.

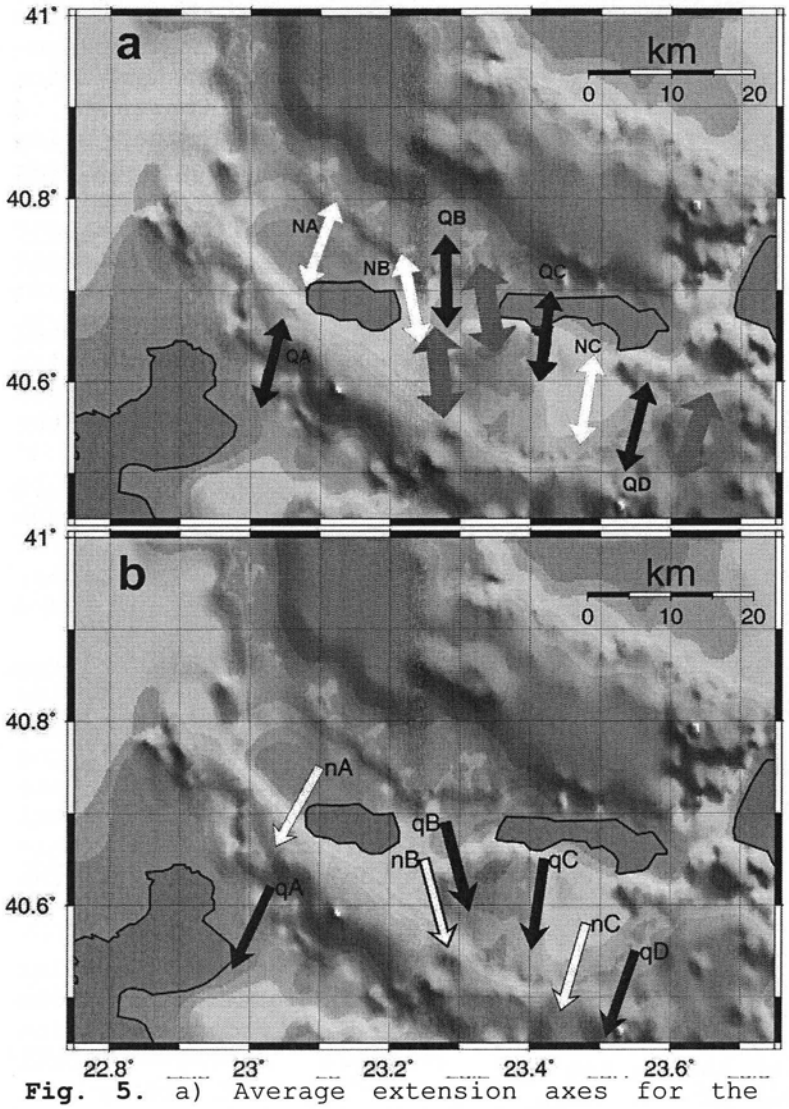

Fig. 5. a) Average extension axes for the small earthquake (black arrows) and the neotectonic (white arrows) data. b) Same as (a) for the average slip vector data.

d) Zone D. This is the area of the 1995/5/4, M_W=5.8, Arnaia mainshock, where both the mainshock as well as the local experiment seismological data show a NNE-SSW extension field, although no neotectonic information were available for this area.

In order to study the behavior of the stress field in each zone, the average "focal mechanism" tensor was estimated for each zone. Figure 5a shows the corresponding extension T-axes defined using the seismological (Q) and neotectonic (N) data. In order to compare the relative motion pattern across the various faults, we also present the average slip vectors, which correspond to the southern hanging wall of the fault plane solution.

The results show an almost identical pattern of the stress-field variation for both data sets. For zone A, a identical NNE-SSW extension field (14°) is found for the two data sets, with an average slip vector direction of 207°. However, both the stress field and the slip-vector directions change for the central part

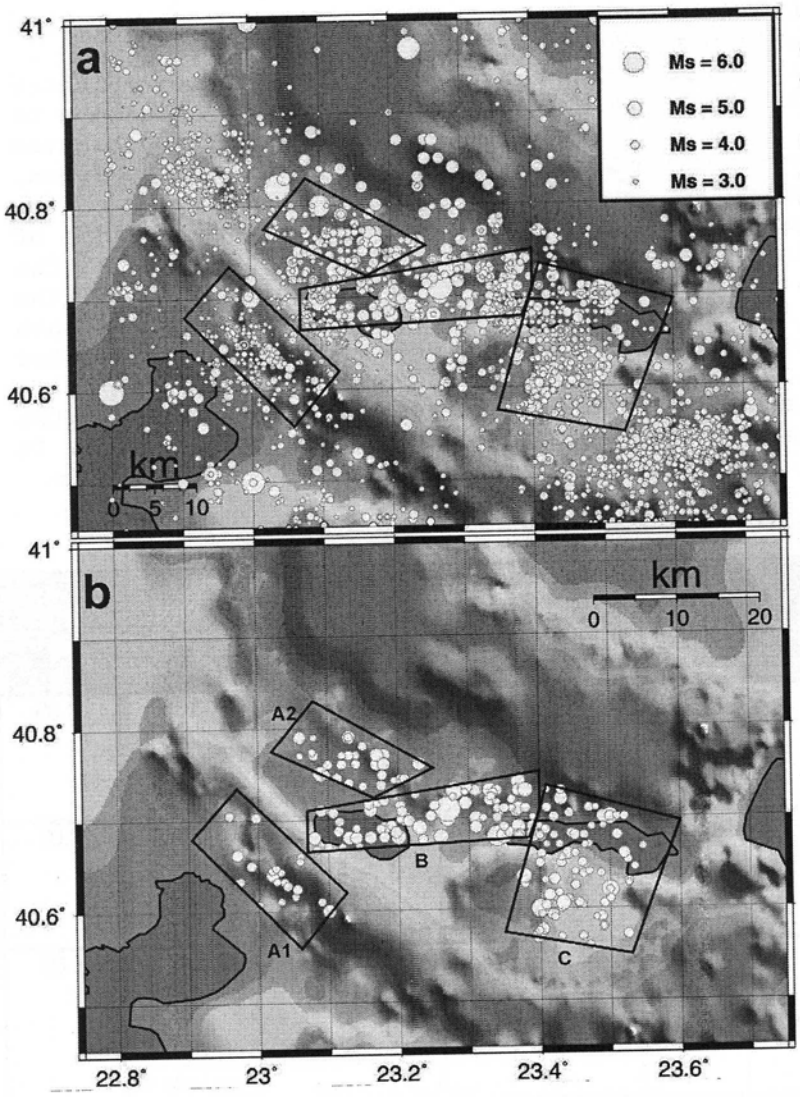

Fig. 6. a) Historical and observed seismicity in the Mygdonia basin area. The studied deformation zones are shown by polygons. b) Same as (a) for the complete seismicity data.

(zone B). The extension axis changes to N-S (359°) for the earthquake data and NNW-SSE (348°) for the neotectonic data, whereas the slip-vectors show an identical SSE (165°) direction. The 1978 preshock and mainshock extension axes are in very good agreement with the proposed T-axis direction. Moving eastward, towards the Volvi area, the extension field changes again to N-S/NNE-SSW (7-9°), with a slightly larger azimuth (14°) in the Arnaia area (zone D) as this is deduced from the seismological data. The slip vectors are also modified in a similar manner, showing a SSW directions between 188° and 199°.

It is interesting to notice that the stress field and the slip vector variations follow the S-shape of the Mygdonia basin. In every zone, the T-axis and especially the slip-vector are almost perpendicular to the basin trend, showing that the geomorphological characteristics are affected but also affect the tectonic regime of the area. Even in areas like zone A, where the stress field is relatively oblique to the basin axis, the basin border faults are still moving away from each other, which suggests that the basin is still under extensive deformation. In the next section we attempt to estimate the deformation rates, using the method previously described.

ESTIMATION OF ACTIVE CRUSTAL DEFORMATION IN THE MYGDONIA BASIN

Figure 6a shows the observed seismicity (historical and instrumental) for the examined area. It is easily seen that most of the seismic activity in the area is concentrated in the Mygdonia basin. The polygons delineate the main zones which have been previously defined and which contains most of the seismic activity in the area. We have selected not to include the Arnaia area (zone D) in the calculations due to the absence of neotectonic information, few fault plane solutions from earthquakes but mostly since the intense recent aftershock activity after the 1995 event would probably result in an overestimation of the deformation rates.

In order to estimate the deformation rate for each source, it is necessary to use only the complete seismicity data. For the study area, we used the completeness derived for the broader Aegean area from Papazachos and Papazachou (1997), in combination with the results of Scordilis (1985) for the Servomacedonian area. Hence, we considered as complete all $M_W \geq 5.0$ events after 1911, $M_W \geq 4.5$ after 1950, $M_W \geq 4.3$ after 1965 and $M_W \geq 3.0$ after 1981. The corresponding distribution of the complete seismicity for the 4 polygonal areas

is shown in figure 6b, where it is clearly seen that the central part is the most active section of the Mygdonia basin system.

Using the complete seismicity data, the parameters of the Gutenberg-Richter relation were calculated. For the moment-rate estimation it is also necessary to define the maximum expected magnitude for each zone. From the observed seismicity (fig. 6a) the maximum observed event was defined in each polygon. Especially for zone A1, although the maximum observed event was M=5.5, the maximum magnitude considered was increased to M_W=6.0, since both the length of the active neotectonic faults in the area, as well as the possibility that the 1759 event is located in this zone suggest that the seismic potential of the zone can produce an event of such magnitude. The information regarding each zone, as well as the determined maximum magnitude and the Gutenberg-Richter parameters are shown in Table 1. In the same table the geometric characteristics of each zone (length, width, azimuth) used in equation (1), as well as the annual moment-rate finally estimated using equation (2) are also presented. In all cases, the thickness of the seismogenic layer was considered equal to 10km.

Table 1. Parameters of the zones for which deformation has been estimated.

ZONE	ZONE LIMITS		COMPLETENESS		MAXIMUM MAGNITUDE	LENGTH	WIDTH	AZIMUTH	ANNUAL MOMENT-RATE	GUTENBERG-RICHTER PARAMETERS	
	φ°N	λ°E	t	Mmin	Mw,max	l1 (km)	l2 (km)	ξ	Mo	a (Annual)	b
A1	40.680	22.905	1911	5.0	5.5	20.6	9.1	134	0.297E+23	3.36	1.05
	40.735	22.970	1950	4.5	6.0						
	40.620	23.125	1965	4.3							
	40.560	23.060	1981	3.0							
A2	40.775	23.020	1911	5.0	5.9	17	7.9	115	0.558E+23	3.58	1.03
	40.830	23.080	1950	4.5							
	40.775	23.250	1965	4.3							
	40.723	23.165	1981	3.0							
B	40.665	23.070	1911	5.0	6.6	30.9	7.9	84	0.598E+24	3.47	0.89
	40.710	23.070	1950	4.5							
	40.750	23.400	1965	4.3							
	40.708	23.400	1981	3.0							
	40.678	23.385									
C	40.735	23.410	1911	5.0	6.6	17.9	20	105	0.253E+24	4.02	1.05
	40.695	23.600	1950	4.5							
	40.550	23.530	1965	4.3							
	40.575	23.350	1981	3.0							

Using the information in Table (1), we proceeded in the determination of the strain and velocity tensors, by the application of equations (1). For this reason the representative focal mechanism tensor was derived for each zone, using the average tensor from both seismological and neotectonic data. The representative fault plane solutions used for each zone are shown in Table 2.

Table 2. Average fault plane solutions of the seismological and neotectonic data of each zone, which were used to determine the average "focal mechanism" tensor.

ZONE		Main Fault Plane		
	Data Type	ζ	δ	λ
A	qA	88	36	-112
	nA	101	43	-102
B	qB	104	45	-68
	nB	82	38	-84
C	qC	96	43	-90
	nC	92	44	-99

Figure 7a shows the horizontal eigenvectors of the velocity tensor determined for each zone using the information presented in Tables 1 and 2. A

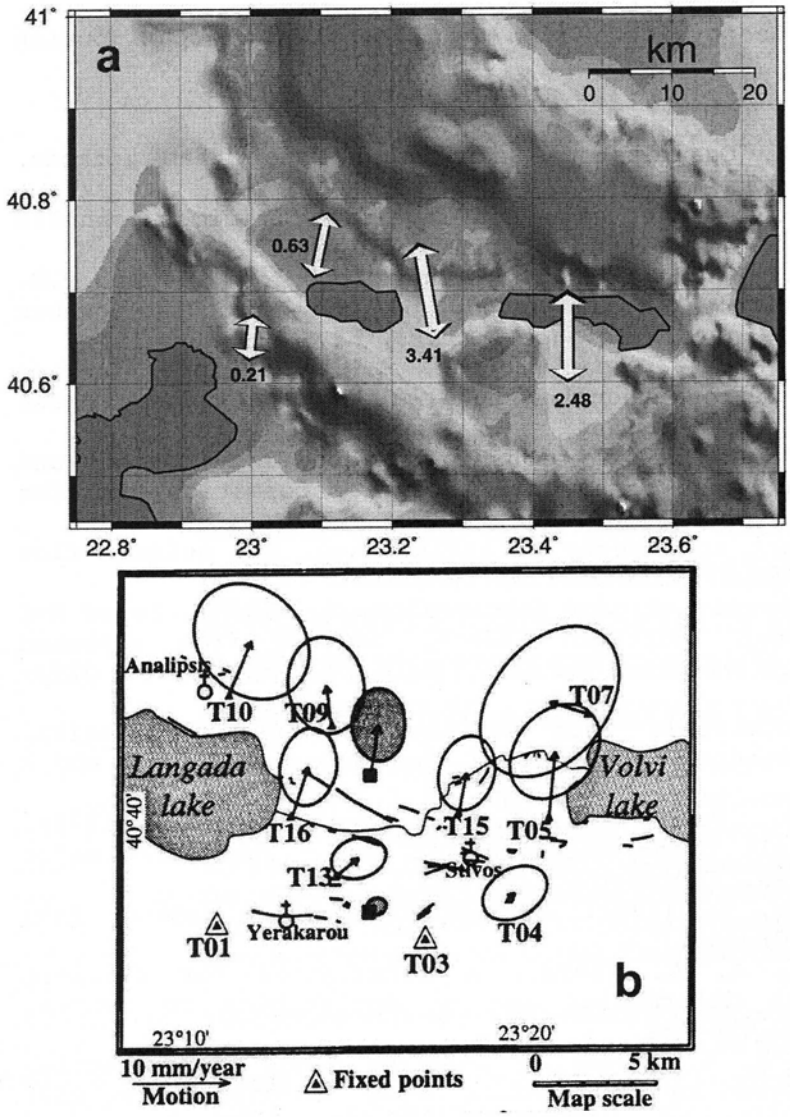

Fig. 7. a) Extensional velocities (in mm/yr) estimated for the studied zones of the Mygdonia basin. b) Velocities of the northern part of the central section of the Mygdonia basin with respect to its southern border, as determined by the use of geodetic data (Martinod et al., 1997).

logarithmic scale is used and the presented velocities are expressed in mm/yr. The results confirm the N-S extensional deformation pattern of the Mygdonia basin area and are in very good agreement with previous large-scale studies (e.g. Papazachos and Kiratzi, 1996). The deformation direction in each zone corresponds very well with the S-shape of the basin, similarly to the stress T-axis and the slip vectors, previously described. Velocities are much higher for the central part of the basin, between the two lakes of Langada and Volvi (~3.5mm/yr) and relatively high for the broader Volvi area (~2.5mm/yr). On the other hand, the deformation velocities at the borders of the western part of the area (zones A1 and A2) exhibit much lower velocities, which correspond very well with the lower seismicity levels of this area. Moreover, in this area (zone A) the Mygdonia basin has its smallest aperture, which suggests that the identified velocity contrast of a factor of ~4 between the western and central-eastern part of the Mygdonia basin has probably also occurred during the last phase of the Mygdonia basin formation and is still going on until today. Furthermore, the corresponding near-vertical thinning rates are 0.31mm/yr for zone A1, 0.81mm/yr for zone A2, 4.6 mm/yr for zone B and 1.2mm/yr for zone C. The high thinning rates for the central part are also in agreement with the location of the lowest topographic depression in the central part of the basin between the two lakes.

Figure 7b presents the determined velocities using GPS and conventional geodetic data of the northern part of the central section of the Mygdonia basin (corresponding to zone B) with respect to stations T01 and T03, located at the southern flank of the central Mygdonia basin (Martinod et al., 1997). It should be noted that the geodetic data exhibit an almost identical N-S extension pattern for the area. The average determined velocity from the geodetic data for the total extension between 1978 and 1994 is equal to 5.7mm/yr. This observation suggests that the seismic (active) crustal deformation is approximately 60% of the total deformation, which is expressed by the geodetic measurements, in agreement with previous results for the broader Aegean area (Papazachos and Kiratzi, 1996).

ACKNOWLEDGEMENTS

This work is a Department of Geophysics, Univ. of Thessaloniki contribution number #0000/2001.

REFERENCES

Aki, K. and Richards, P. (1980). Quantitative Seismology: Theory and methods, Freeman, San Francisco, Calif.,557 pp.

Christodoulou, A. (1986). Etude Sismotectonique et Inversion Tridimensionnelle en Grece du Nord. PhD thesis, University of Grenoble I, pp. 181.

Hatzfeld, D., Christodoulou, A.A., Scordilis, E.M., Panagiotopoulos, D., and P.M. Hatzidimitriou, (1987). A microearthquake study of the Mygdonian graben (northern Greece). *Earth and Planetary Science Letters,* 81, 379-396.

Hatzidimitriou, P.M., Scordilis, E.M., Papadimitriou, E.E., Hatzfeld, D. and Christodoulou, A.A. (1991). Microearthquake study of the Thessaloniki area (northern Greece). *Terra Nova,* 3, 648-654.

Jackson, J. and McKenzie, D. (1988). The relationship between plate motions and seismic moment tensors and the rates of active deformation in the Mediterranean and Middle East. *Geophys. J. Int.*, 93, 45-73.

Kostrov, V. (1974). Seismic moment and energy of earthquakes, and seismic flow of rock. *Izv. Acad. Sc. USSR Phys. Solid Earth*, 1, 23-44.

Martinod, J., Hatzfeld, D., Savvaidis, P. and Katsambalos, K. (1997). Rapid N-S extension in Mygdonian graben (Northern Greece) deduced from repeated geodetic surveys. *Geophysicals Research Letters,* Vol. 24, No. 24, p. 3293-3296.

Mountrakis et al. (1997). Neotectonic Maps of Langada and Thessaloniki, Laboratory of Geology and Paleontology, Univ. of Thessaloniki, 2 maps and 2 leaflets.

Papazachos, B.C., Mountrakis, D., Psilovikos, A. and Leventakis, G. (1979). Surface fault traces and fault plane solutions of May - June 1978 major shocks in the Thessaloniki area. *Tectonophysics*, 53, 171-183.

Papazachos, B. C. and Papazachou, K. (1997). The earthquakes of Greece, *Ziti Publ.*, 304pp., Thessaloniki, Greece.

Papazachos, C. B. and Kiratzi, A. A. (1992). A formulation for reliable estimation of active crustal deformation and an application to central Greece. *Geophys. J. Int.*, 111, 424-432.

Papazachos, C. B., and Kiratzi, A. A. (1996). A detailed study of the active crustal deformation in the Aegean and surrounding area, *Tectonophysics*, 253, 129-153.

Papazachos, C., Soupios, P., Savvaidis, A. and Roumelioti, Z. (2000). Identification of small-scale active faults near metropolitan areas: an example from the Asvestochori fault near Thessaloniki, *Proc. Of the XXVII ESC General Assembly, Lisbon, Portugal, 15-20 September 2000*, (in press).

Pavlidis, S.B. and Kilias, A.A. (1987). Neotctonic and active faults along the Servomacedonian zone (SE Chalkidiki, northern Greece). *Annales Tectonicae,* Vol. I, n. 2, 9-104.

Pavlides, S.B., Kondopoulou, D.P., Kilias, A.A. and Westphal, M. (1988). Complex rotational deformations in the Serbo-Macedonian massif (north Greece): structural and palaeomagnetic evidence. *Tectonophysics,* 145, 329-335.

Scordilis, E.M., (1985). Microseismic study of the Servomacedonian zone and the surrounding area. *Ph.D. Thesis,* University of Thessaloniki, (in Greek).

Geophysical Research Abstracts, Vol. 5, 08794, 2003

STRESS-FIELD AND TIME-VARIATION OF ACTIVE CRUSTAL DEFORMATION IN THE MYGDONIA BASIN BASED ON THE JOINED INTERPRETATION OF SEISMOLOGICAL, NEOTECTONIC AND GEODETIC DATA

Vamvakaris D.A. (1), Papazachos C.B. (1), Savvaidis P.D. (2), Tziavos I.N. (3), Karagianni E.E. (1), Skordilis E.M. (1) and Hatzidimitriou P.M. (1)

(1) Dept. of Geophysics, School of Geology, Aristotle University of Thessaloniki, PO Box 352-1, Thessaloniki, GR-54124, GREECE [dom@lemnos.geo.auth.gr /fax:+2310-998528], (2) Dep. of Civil Engineering, Lab. of Geodesy, Aristotle University of Thessaloniki, Univ.Box. 465, GR-54124 Thessaloniki, GREECE, (3) Dep. of Geodesy and Surveying, Aristotle University of Thessaloniki, Univ.Box 440, Thessaloniki, GR-54124, GREECE

In the present work we examine the active tectonics setting and related deformation scheme in the Mygdonia basin (N. Greece), on the basis of the joint interpretation of seismological and neotectonic data. In order to determine its spatial distribution we studied the stress-field derived from fault plane solutions of small-magnitude events from a local seismological experiment, as well as neotectonic observations. The results show an almost identical spatial variation of the stress field determined from the two independent data sets, which also exhibits a very good correlation with the geomorphological changes in the Mygdonia basin. Moreover, the average stress field is almost identical to the corresponding stress pattern determined from the 3 largest events in the study area for which reliable fault plane solutions are available. Moreover, geodetic data collected by a local network established in this area are also used. This data represent the crustal deformation of the studied area for the last 23 years. The active crustal deformation is studied for the most active sections of the Mygdonia basin system, using the combined stress pattern and the corresponding moment-rate tensors derived from both seismological and neotectonic data sets. The results show a N-S extension at an average rate of 3mm/yr for the central part of the Mygdonia sys-

tem, in very good agreement with the available geodetic results. The time-variation of the active crustal deformation is also studied. Seismicity levels after the mainshock of the 20th of June 1978 are in good agreement with the mean values for the whole century, as is shown from the time-distribution of both moment-rate and deformation. Moreover a significant reduction of these values is detected for the last 10 years, in agreement with geodetic data. We have also performed a stress-tensor inversion in order to examine whether the stress field related with the earthquakes and the neotectonic observations of our dataset is in agreement with the results of the geodetic experiments, using the method of Gephart and Forsyth (1984). Applying the method for the seismological data, the main fault plane related to each earthquake and the mean stress field for the area of study have been determined. The application using the neotectonic data produces a similar stress field pattern. The results show a good agreement of the stress-field derived from the fault plane solutions, as well as neotectonic observations with the stress-field derived from the stress-tensor inversion and the geodetic data. However the stress-tensor inversion is able to identify the correct fault plane in only 2/3 of the examined cases for the neotectonic data.

STRESS-FIELD AND TIME-VARIATION OF ACTIVE CRUSTAL DEFORMATION IN THE MYGDONIA BASIN BASED ON THE JOINED INTERPRETATION OF SEISMOLOGICAL, NEOTECTONIC AND GEODETIC DATA

Vamvakaris D.A.*, Papazachos C.B.*, Savvaidis P.D.**, Tziavos I.N.***, Karagianni E.E.*, Scordilis E.M.* & Hatzidimitriou P.M.*

* Geophysical Laboratory, Aristotle University of Thessaloniki, Thessaloniki, Greece
** Dep. of Civil Engineering, Lab. of Geodesy, Aristotle University of Thessaloniki, Thessaloniki, Greece
*** Dep. Of Geodesy and Surveying, Aristotle University of Thessaloniki, Thessaloniki, Greece

ABSTRACT

In the present work we examine the active tectonics setting and related deformation scheme in the Mygdonia basin (N. Greece), on the basis of the joint interpretation of seismological, neotectonic and geodetic data. In order to determine its spatial distribution we studied the stress-field derived from fault plane solutions of small-magnitude events from a local seismological experiment, as well as neotectonic observations. Additional, geodetic data collected by a local network established in this area are also used. This data represent the crustal deformation of the studied area for the last 23 years. The active crustal deformation is studied for the most active sections of the Mygdonia basin system, using the combined stress pattern and the corresponding moment-rate tensors derived from both seismological and neotectonic data sets.

The time-variation of the active crustal deformation is also studied. Seismicity levels after the mainshock of the 20th of June 1978 are in good agreement with the mean values for the whole century, as is shown from the time-distribution of both moment-rate and deformation. Moreover a significant reduction of these values is detected for the last 10 years, in agreement with geodetic data.

A stress-tensor inversion has been also performed in order to examine whether the stress field related with the earthquakes and the neotectonic observations of our dataset is in agreement with the results of the geodetic experiments.

Fig.1. Main geological zones of Greece. The inset figure shows the Mygdonia basin area.

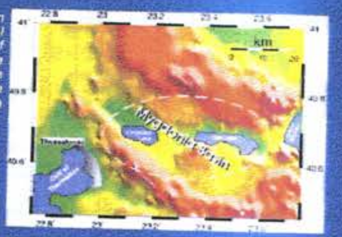

Fig.2. Geomorphological map of the broader Mygdonia basin area.

DATA USED

Seismological Data

The first data set (fig. 3A) corresponds to the fault plane solutions determined from the analysis of earthquakes recorded by a local network which operated in the Mygdonia area in the spring of 1984 and 1985 (Christodoulou, 1986; Hatzfeld et al., 1987). Additional fault plane solutions for the Asvestochori area were used from the work of Papazachos et al. (2000).

Neotectonic Data

The second dataset corresponds to the neotectonic faults and related information reported in the neotectonic maps of "Langadas" and "Thessaloniki" (Mountrakis et al., 1997). The corresponding fault plane solutions are also shown (fig.3B).

Geodetic Data

The last set of data corresponds to the geodetic measurements using a local geodetic network of 16 points witch is established in the central part of the basin (between the two lakes) since 1979. In the present work only the 10 out of 16 points of the 1979's network are used, taking under consideration also the results of GPS measurements of 1994 (Martinod et al., 1997) and 1997 experiments.

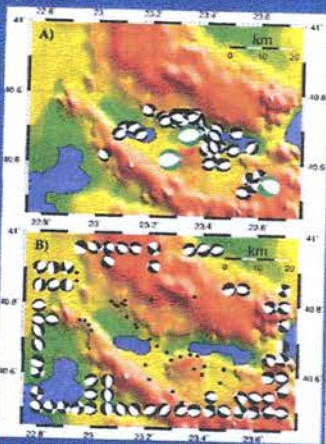

Fig.3. A) Fault plane solutions determined for 63 small earthquakes recorded in 1984 and '85 (black solutions). The solutions of the 3 main earthquakes (M_s>5.5) are also shown (green solutions). B) Fault plane solutions corresponding to the neotectonic faults of the broader Mygdonia basin.

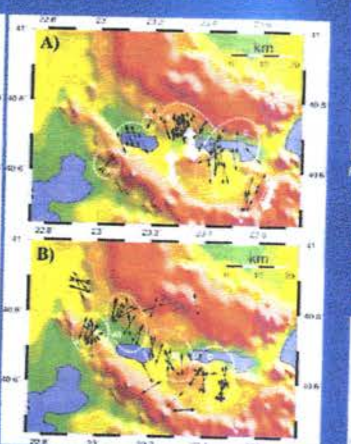

Fig.4. A) Extensional T-axes for the 63 small earthquakes (black arrows) and the 3 main events with M_s>5.5 (white arrows), grouped in zones with similar tectonic characteristics. B) Same as (A) for the neotectonic data.

METHOD

We applied the method of Papazachos and Kiratzi (1992), which is based on the results of Kostrov (1974) and Jackson and McKenzie (1988) and relies on the use of all complete seismicity data for the estimation of the size of the deformation and all the available fault plane solutions, which do not need to be complete for the examined time period. Using this approach, the problem of complete fault plane solution data can be overcome, using information derived from other sources. For the estimation of the strain rate tensor, $\dot{\varepsilon}_{ij}$, and the velocity tensor, U_{ij}, the following equations (1) and (2) are used (Papazachos and Kiratzi, 1992).

[illegible] (1)

[illegible] (2)

[illegible] (3)

Where
H1, H2, H3: zone dimensions
μ: shear modulus
$\dot{M}_o$: released moment-rate
$M_{o,max}$: seismic moment of the max event in the zone
A, B: constants

$\dot{M}_o$, is the released moment rate which is defined by the seismicity level of the area, using the relation (3) of Molnar (1979). $\bar{F}$ is the average "focal mechanism" tensor, representing the deformation pattern of the area and is the average of the individual F tensors, corresponding to each fault plane solution and are a function of the corresponding strike, ζ, dip, δ, and rake, λ (Aki & Richards, 1980).

IDENTIFICATION OF ZONES

In order to define zones of similar tectonic setting, the spatial distribution of the T-axes was studied, since the area is dominated by extension. Four main zones were recognized (fig. 4), for which the average "focal mechanism" tensor was estimated.

The results show an almost identical pattern of the stress-field variation for both data sets (fig.5). It is interesting to notice that the stress field and the

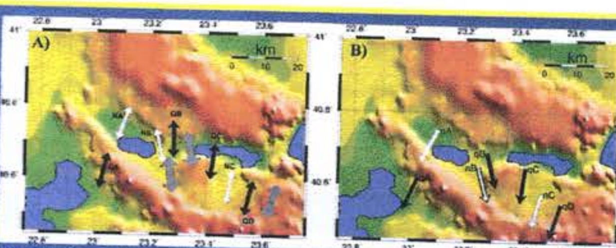

Fig.5. A) Average T-axes for the small earthquakes (black arrows) and the neotectonic data (white arrows). T-axis for the 3 main earthquakes (gray arrows) are also shown. B) Same as (A) for the average slip vector.

Mygdonia basin, as both the T-axis and the slip-vector are almost perpendicular to the basin trend, showing that the geomorphological characteristics are affected by the tectonic regime of the area.

STRESS TENSOR INVERSION

To confirm the similarity of the results produced by the use of seismological and neotectonic data, we performed a stress-tensor inversion, using the method of Gephart & Forsyth (1984). Applying the method for the seismological data, we have chosen the planes corresponding to the minimum misfit rotation about any axis of general orientation which is needed to match an observed fault plane/slip direction with one consistent with the given stress model. The main fault plane related to each earthquake and the mean stress field for the area of study have been determined. The application using the neotectonic data produces a similar stress field pattern.

The results show a good agreement of the stress-field derived from the fault plane solutions, as well as neotectonic observations with the stress-field derived from the stress-tensor inversion and the geodetic data. However the stress-tensor inversion is able to identify the correct fault plane in about 70% of the examined cases for the neotectonic data (fig. 6).

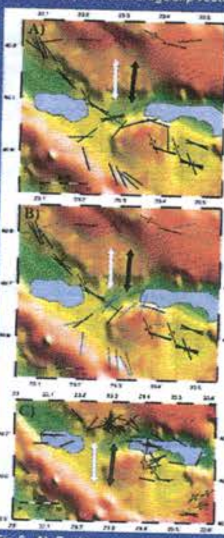

Fig.6. A) Faults corresponding to the neotectonic observations. B) Ideal fault planes with the minimum misfit rotation, according to the inversion method. Black and blue lines correspond to fault observed and not observed in the field, respectively. C) Selected fault planes corresponding to the seismological data, using the inversion method. Mean T-axis for neotectonic (white) and seismological (black) data are also shown.

ESTIMATION OF CRUSTAL DEFORMATION

We have focused in the central part of the Mygdonia basin, where a geodetic network was established in 1979. The velocities derived between 1979 and 1997 on the basis of conventional geodetic and GPS data confirm the ~N-S basin extension, showing a rate of 5.7mm/yr between stations located in the south and north basin margins (fig. 7A,B). In order to compare with seismological estimates we used the complete seismicity data and the parameters of the Gutenberg-Richter relation were calculated, assuming a maximum expected magnitude of M_w=6.6, using the available historical information.

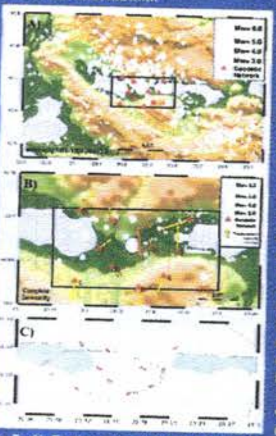

Fig.7. A) Earthquakes with M_s≥3.0 for the years 1978-99, in the broader area of study. Geodetic network is also shown. B) Geodetic network and complete seismicity for the years 1978-99 in the examined area. Stations and average velocities are also shown (mm/yr). C) Maximum shear stress (arbitrary units) derived from geoid anomalies and elasticity theory. Notice the large shear stress between the two lakes.

The a & b parameters were estimated for the last century (1911-2000). 3 year period-values for the annual parameters were also estimated for the years 1977-1999 and 22 a-b pairs of parameters were produced (b was kept constant corresponds to the whole century value).

The results (fig. 8) were compared with the geodetic information for the same area. Large values for the year 1978, clearly related with the major earthquake of Thessaloniki (20/6/78, M_s=6.5) are shown. This is confirmed by interpretation of geoid anomalies using the elasticity theory (fig.7C), which shows large shear stress in the area between the two lakes (Tziavos and Andritsanos, 1999). For the next 10-12 years deformation seems to be "normal", in agreement with the average 20^{th} century level. After 1990, deformation and moment-rate release appears to be continuously decreasing until 2000, when the estimated moment-rate is one order of magnitude smaller than the average.

Concerning the deformation rates, the mean horizontal velocity is 0.58 cm/yr (for the whole century) with a 174° direction, while the vertical rate is almost double, in good agreement with the results produced using the geodetic data (0.57 cm/yr) since 1978. After 1979 deformation is almost constant (0.5-1.0 cm/yr) with values similar to the average calculated. This situation changes after 1990 where the deformation seams to be continuously decreasing until 2000.

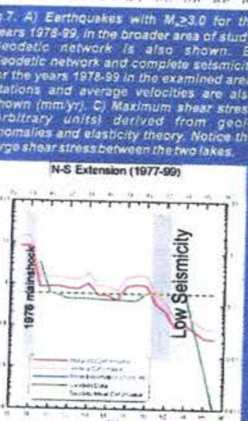

Fig.8. Time variation of deformation velocities using seismological and geodetic data. Notice the similarity of the time variation of the two data sets.

CONCLUSIONS

Both seismological and neotectonic results show a N-S extension at an average rate of ~6 mm/yr for the central part of the Mygdonia basin, in very good agreement with the available geodetic results. Deformation in the examined area since 1978 seams to be normal with values similar to the mean 20^{th} century value. However, after 1990 a continuous decrease is observed until present, where both moment-rate and deformation have values almost one order of magnitude less than the average.

A stress tensor inversion confirmed that the stress field related with the earthquakes and the neotectonic observations of our dataset is in agreement with the results of the geodetic experiments. However, selection of the main fault plane for geodetic data using the minimum rotation misfit between the shear stress and the fault slip was able to identify the observed neotectonic faults in ~70% of the examined cases. This result indicates that identification of main fault planes using the method of Gephart and Forsyth (1984) should be applied with care.

Acknowledgements

This work was partly supported by the Earthquake Planning and Protection Organization of Greece (E.P.P.O.), projects #20237 and #20321, Res. Com. Univ. Of Thessaloniki.

References

Aki, K. and Richards, P. (1980). Quantitative Seismology: Theory and methods. *Freeman, San Francisco, Calif. 557pp.*
Christodoulou, A. (1986). Etude Sismotectonique et Inversion Tridimensionnelle en Grece du Nord. *PhD thesis, University of Grenoble I, pp. 181.*
Gephart, J. W. and Forsyth, D. W. (1984). An improved method for determining the regional stress tensor using earthquake focal mechanism data: Application to the San Fernando earthquake sequence. *Jour. of Geophysical Res., Vol. 89, No. B11, p. 9305-9320.*
Hatzfeld, D., Christodoulou, A.A., Scordilis, E.M., Panagiotopoulos, D., And P.M. Hatzidimitriou. (1987). A microearthquake study of the Mygdonian graben (northern Greece). *Earth and Planetary Science Letters, 81, 379-396.*
Jackson, J. and McKenzie, D. (1988). The relationship between plate motions and seismic moment tensors and the rates of active deformation in the Mediterranean and Middle East. *Geophys. J. Int., 93, 45-73.*
Kostrov, V. (1974). Seismic moment and energy of earthquakes, and seismic flow of rock. *Izv. Acad. Sci. USSR Phys. Solid Earth, 1, 23-44.*
Martinod, J., Hatzfeld, D., Savvaidis, P. and Katsambalos, K. (1997). Rapid N-S extension in Mygdonian graben (Northern Greece) deduced from repeated geodetic surveys. *Geophysicals Research Letters, Vol. 24, No. 24, p. 3293-3296.*
Mountrakis et al. (1997). Neotectonic Maps of Langada and Thessaloniki. *Lab. of Geology and Paleontology, Univ. of Thessaloniki, 2 maps and 2 leaflets.*
Papazachos, C. B. and Kiratzi, A. A. (1992). A formulation for reliable estimation of active crustal deformation and an application to central Greece. *Geophys. J. Int., 111, 424-432.*
Papazachos, C., Soupios, P., Savvaidis, A. and Roumelioti, Z. (2000). Identification of small-scale active faults near metropolitan areas: an example from the Asvestochori fault near Thessaloniki. [illegible]

PERGAMON

Journal of Structural Geology xx (0000) xxx–xxx

JOURNAL OF STRUCTURAL GEOLOGY

www.elsevier.com/locate/jsg

Thessaloniki–Gerakarou Fault Zone (TGFZ): the western extension of the 1978 Thessaloniki earthquake fault (Northern Greece) and seismic hazard assessment

Markos D. Tranos[a,*], Eleftheria E. Papadimitriou[b], Adamantios A. Kilias[a]

[a]*Department of Geology and Palaeontology, University of Thessaloniki, GR-54124 Thessaloniki, Greece*
[b]*Geophysics Department, University of Thessaloniki, GR-54124 Thessaloniki, Greece*

Received 31 October 2001; received in revised form 1 August 2002; accepted 17 February 2003

Abstract

Active faulting and seismic properties are re-investigated in the eastern precinct of the city of Thessaloniki (Northern Greece), which was seriously affected by two large earthquakes during the 20th century and severe damage was done by the 1759 event. It is suggested that the earthquake fault associated with the occurrence of the latest destructive 1978 Thessaloniki earthquake continues westwards to the 20-km-long Thessaloniki–Gerakarou Fault Zone (TGFZ), which extends from the Gerakarou village to the city of Thessaloniki. This fault zone exhibits a constant dip to the N and is characterised by a complicated geometry comprised of inherited 100°-trending faults that form multi-level branching (tree-like fault geometry) along with NNE- to NE-trending faults. The TGFZ is compatible with the contemporary regional N–S extensional stress field that tends to modify the pre-existing NW–SE tectonic fabric prevailing in the mountainous region of Thessaloniki. Both the 1978 earthquake fault and TGFZ belong to a ca. 65-km-long E–W-trending rupture fault system that runs through the southern part of the Mygdonia graben from the Strymonikos gulf to Thessaloniki. This fault system, here called Thessaloniki–Rentina Fault System (TRFS), consists of two 17–20-km-long left-stepping 100°-trending main fault strands that form underlapping steps bridged by 8–10-km-long ENE–WSW faults. The occurrence of large ($M \geqq 6.0$) historical earthquakes (in 620, 677 and 700 A.D.) demonstrates repeated activation, and therefore the possible reactivation of the westernmost segment, the TGFZ, could be a major threat to the city of Thessaloniki. Changes in the Coulomb failure function (ΔCFF) due to the occurrence of the 1978 earthquake calculated out in this paper indicate that the TGFZ has been brought closer to failure, a convincing argument for future seismic hazard along the TGFZ.

Keywords: Active faulting; Seismic activity; Fault segmentation; Earthquake triggering; Coulomb stress; Thessaloniki; Northern Greece

1. Introduction

Destructive earthquakes occurring close to populated areas demonstrate the necessity of additional efforts to improve existing scientific knowledge on active faulting and its relationship with the seismicity in the area of interest, the ultimate goal being the assessment of the future seismic hazard. Many attempts have been made in seismically active areas to evaluate the behaviour of the earthquake faults and the possible occurrence of earthquakes on neighbouring faults, taking into account fault interaction. Faults are not mechanically isolated structures, but they occur within a population of faults and they may interact with other faults through their stress field. Many recent earthquake sequences involved slip on interacting fault segments showing that fault interaction can profoundly affect rupture sequences, such as in the case of the 1999 Izmit and Duzce mainshocks (Hubert-Ferrari et al., 2000; Parsons et al., 2000; Papadimitriou et al., 2001).

This study refers to the Thessaloniki area, which has recently been affected by the 1978 destructive earthquake sequence (Papazachos and Papazachou, 1997). Since then, an intense neotectonic and seismological investigation of the broader area has been carried out (Papazachos et al., 1979, 1982; Mercier et al., 1983; Mountrakis et al., 1983, 1996; Hatzfeld et al., 1987; Pavlides and Kilias, 1987; Pavlides et al., 1990; Tranos, 1998). The results contribute to the better understanding of the active faulting and seismicity of the study area. However, the identification and

* Corresponding author. Tel./fax: +30-310-998482.
E-mail address: tranos@geo.auth.gr (M.D. Tranos).

0191-8141/03/$ - see front matter © 2003 Elsevier Science Ltd. All rights reserved.
doi:10.1016/S0191-8141(03)00071-3

geometry of the seismic fault of the 1978 earthquake, its behaviour within the regional fault pattern, and its probable future reactivation need further investigation. Therefore, the fault geometry and more precisely the length, orientation and extension of the 1978 Thessaloniki earthquake fault are among the targets of the present study. The Coulomb stress changes due to the 1978 seismic sequence are also calculated to identify which other faults, or fault segments are currently in stress-enhanced areas, and to evaluate the future seismic hazard in the study area.

2. Geology and seismotectonic setting

The broader Thessaloniki area lies in Central Macedonia and constitutes part of the Inner Hellenic orogen (Fig. 1). The exposed rocks forming the pre-alpine and alpine basement belong to the NNW–SSE-trending alpine Circum Rhodope Belt Thrust System (CRBTS), which is characterized by several NE-dipping asymmetric anticlinoria and synclinoria and repeated SW-directed thrust sheets (Tranos et al., 1999). Above this basement extensive NW–SE- and E–W-trending continental-type basins and grabens have been filled with Neogene and Quaternary sediments. They were developed by a Miocene to present extensive brittle extensional deformation that mainly related to high-angle normal faults (Pavlides and Kilias, 1987; Tranos, 1998; Tranos et al., 1999). Among these basins the E–W-trending Mygdonia graben and its preceding NW–SE Pre-Mygdonia basin are directly related to our study as they formed at the northern slopes of the mountainous area of Thessaloniki. This extensional deformation has the least principal stress axis (σ_3) oriented NE–SW in Late Miocene–Pliocene and N–S since Quaternary (Pavlides and Kilias, 1987; Mercier et al., 1989; Pavlides et al., 1990; Tranos, 1998; Tranos and Mountrakis, 1998) and forms a back-arc, with the extension related to the Hellenic subduction zone (Angelier, 1979; Mercier, 1981).

The fault pattern of the broader area is rather complicated, including NW–SE-, NE–SW-, E–W- and NNE–SSW-trending faults. Many of them are inherited structures active at least since the Miocene (Pavlides and Kilias, 1987; Pavlides et al., 1990; Tranos, 1998; Tranos and Mountrakis, 1998; Tranos et al., 1999), whereas the E–W-trending faults are associated with the seismic activity or have verified Quaternary activity (Mountrakis et al., 1996; Tranos, 1998). However, the faults affecting the basement exhibit complicated kinematics usually with more than one slickenline on their surfaces (Pavlides et al., 1990; Tranos, 1998).

The study area is characterised by intense seismic activity with strong earthquakes of magnitudes up to M = 7.0 from historical times to the present (Fig. 2; Table 1, data from Papazachos and Papazachou, 1997). More

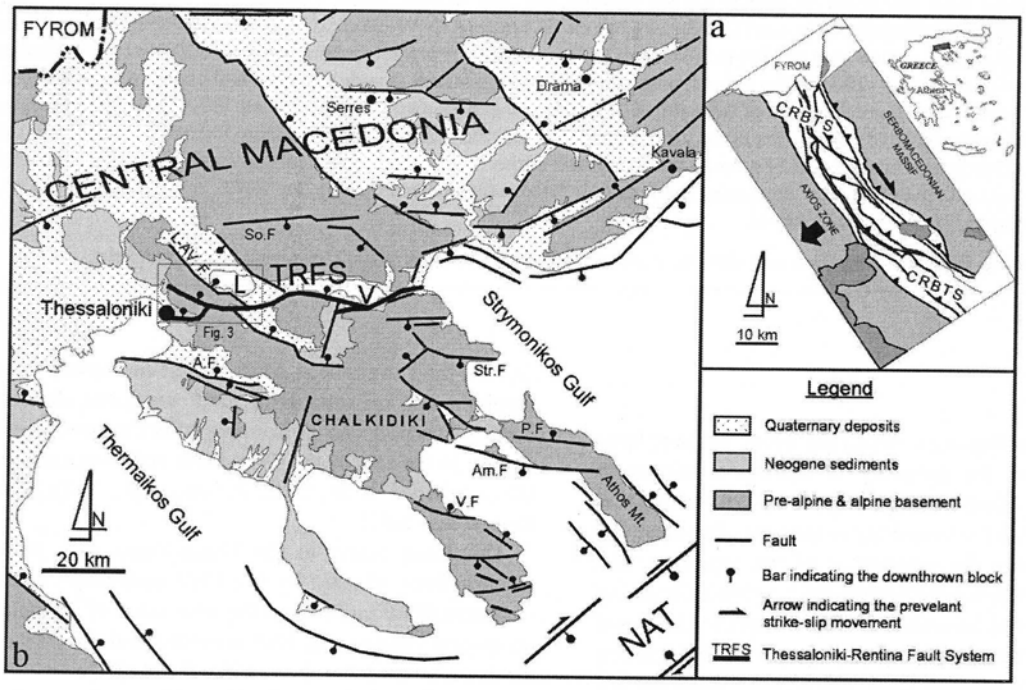

Fig. 1. Generalised geological and tectonic map showing the Thessaloniki–Rentina Fault System and its westernmost part, the Thessaloniki–Gerakarou Fault Zone, in the fault-dominated area of Central Macedonia. Am. F: Amoliani Fault, A. F: Anthemountas Fault, L–AV. F: Lagina–Ag. Vasilios Fault, P. F: Pirgos Fault, So. F: Sochos Fault, Str. F: Stratoni Fault, V. F: Vourvourou Fault, L: Langadas Lake, V: Volvi Lake. The inset map in the upper right corner shows the transpressive Circum Rhodope Belt Thrust System that dominates the deformation of the pre-Alpine and Alpine basement rocks from Oligocene to Miocene times (modified from Tranos et al., 1999) and the position of the studied area in the Greek mainland (Fig. 2).

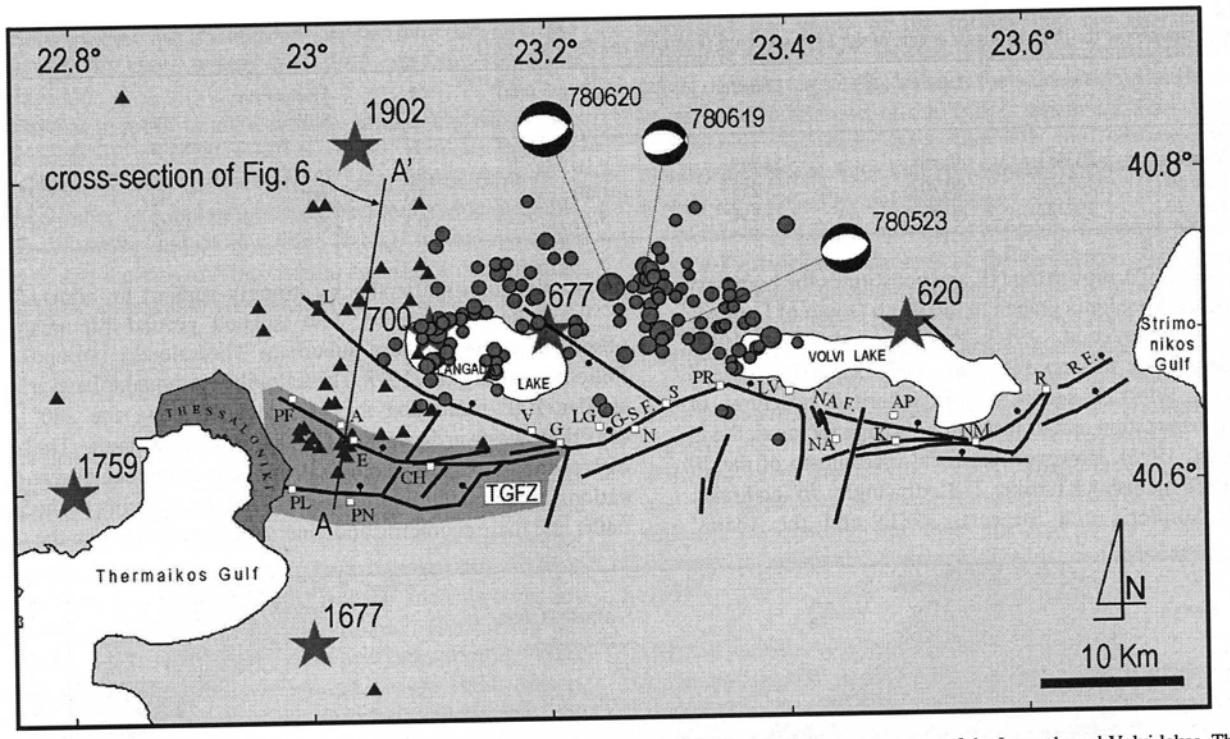

Fig. 2. Map showing the seismic activity of the broader Thessaloniki area and the main faults along the southern part of the Langada and Volvi lakes. The studied TGFZ is indicated in the dark grey frame. Stars are the epicentres of the historically known strong ($M > 6.0$) earthquakes. Focal mechanisms correspond to the main earthquakes of the 1978 sequence (see Table 2). Aftershocks spatial distribution (solid circles) of the 1978 seismic sequence (data from Carver and Bollinger, 1981) and epicentres of the June 1999 sequence (solid triangles) recorded by a dense portable network (Papazachos et al., 2000) are also shown. The A–A′ straight thin line denotes the cross-section shown in Fig. 6. Villages: PL: Pilea, PN: Panorama, PF: Pefka, A: Asvestochori, E: Exochi, CH: Chortiatis, V: Vasiloudi, G: Gerakarou, LG: Laghadikia, N: Nikomidino, S: Stivos, PR: Peristerona, LV: Loutra Volvis, NA: Nea Apollonia, AP: Apollonia, K: Kokalou, NM: Nea Madytos, R: Rentina, L: Lagina.

precisely, during the present century two destructive earthquakes, the Assiros (5 July 1902, $M = 6.5$) and Thessaloniki (20 June 1978, $M = 6.5$) occurred in the broader area of Thessaloniki along the E–W Mygdonia graben. The Thessaloniki earthquake sequence (Table 2) is comprised of the larger foreshock on May 23 ($M = 5.3$), the mainshock on June 20 ($M = 6.5$) and the larger aftershock on July 4 ($M = 5.0$). The mainshock caused extensive damage and loss of life in the metropolitan area of Thessaloniki and the surrounding villages.

The most recent seismic activity close to the city of Thessaloniki occurred in the central part of Mt. Chortiatis in the summer of 1999 with the largest event of $M = 3.7$ on June 29. The shocks of this sequence were located in the area containing Asvestochori, Panorama and Chortiatis villages and were felt throughout the whole Thessaloniki area (Papazachos et al., 2000).

Table 1
Strong ($M > 6.0$) earthquakes in the study area since 500 A.D. For the historical events, epicentres are the centres of the rupture zones determined by macroseismic information and M is equivalent moment magnitude (Papazachos and Papazachou, 1997)

Year	Month	Date	Time	ψ_N^0	λ_E^0	M	Reported intensity
620				40.700	23.500	7.0	Thessaloniki (VII)
677				40.700	23.200	6.5	Thessaloniki (VII)
700				40.700	23.100	6.6	Thessaloniki (VII)
1677				40.500	23.000	6.2	Vassilika (VIII)
1759	June	22		40.600	22.800	6.5	Thessaloniki (IX)
1902	July	5	14:56:30	40.820	23.040	6.6	Assiros (IX)
1978	June	20	20:03:21	40.728	23.253	6.5	Stivos (VIII +)

3. The Thessaloniki–Gerakarou Fault Zone (TGFZ)

The ground ruptures observed during the 1978 Thessaloniki sequence (Papazachos et al., 1979) do not identify a unique fault line; instead they delineate three main fracture lines. The most prominent one has an ENE–WSW strike and a length of about 12 km, starting from Peristerona village, passing through Stivos and Nikomidino villages and terminating abruptly to the west of Gerakarou village (Fig. 3). It is aligned along the ENE–WSW (70–80°)-trending Gerakarou–Stivos fault cutting either alluvial deposits or the basement at the south edge of the Mygdonia graben, and it is considered as the surficial trace of the main seismic fault associated with the 1978 Thessaloniki earthquake (Papazachos et al., 1979; Mountrakis et al., 1983).

The Gerakarou–Stivos fault is considered to extend westwards to the Lagina–Ag. Vasilios fault that strikes

Table 2
Source parameters of the three strongest events of the 1978 sequence (Soufleris and Stewart, 1981)

Date	Time	Latitude (ψ_N^0)	Longitude (λ_E^0)	Depth (km)	M	Mechanism Strike	Dip	Rake
1978, May 23	233411	40.698	23.295	6	5.8	265	40	−83
1978, June 19	103106	40.707	23.258	10	5.3	281	44	−66
1978, June 20	200322	40.729	23.254	6	6.5	278	46	−70

NW–SE (130°), dips to the NE and constitutes the boundary fault of the Mygdonia graben to the south (south of Langada Lake) (Mercier et al., 1983; Pavlides and Kilias, 1987; Pavlides, 1993; Mountrakis et al., 1996; Chatzipetros and Pavlides, 1998). It seems to join inherited structures of various orientation and to form an arc shape facing to the N (Pavlides, 1993). However, the focal mechanism of the 20 June 1978 mainshock (strike: 278°, dip angle: 46° and rake: −70°, Soufleris and Stewart, 1981) and the spatial distribution of its aftershocks strongly support an almost E–W strike. In addition, few isolated ground ruptures observed in the northern suburb of Thessaloniki (around Polichni) during the 1978 Thessaloniki earthquake have a similar 100° trend and they are located along the 280° direction westwards of the Gerakarou–Stivos fault. The discrepancy between geological and seismological observations triggered our interest to carry out the mapping of the faults and their geometric and kinematical analysis from the

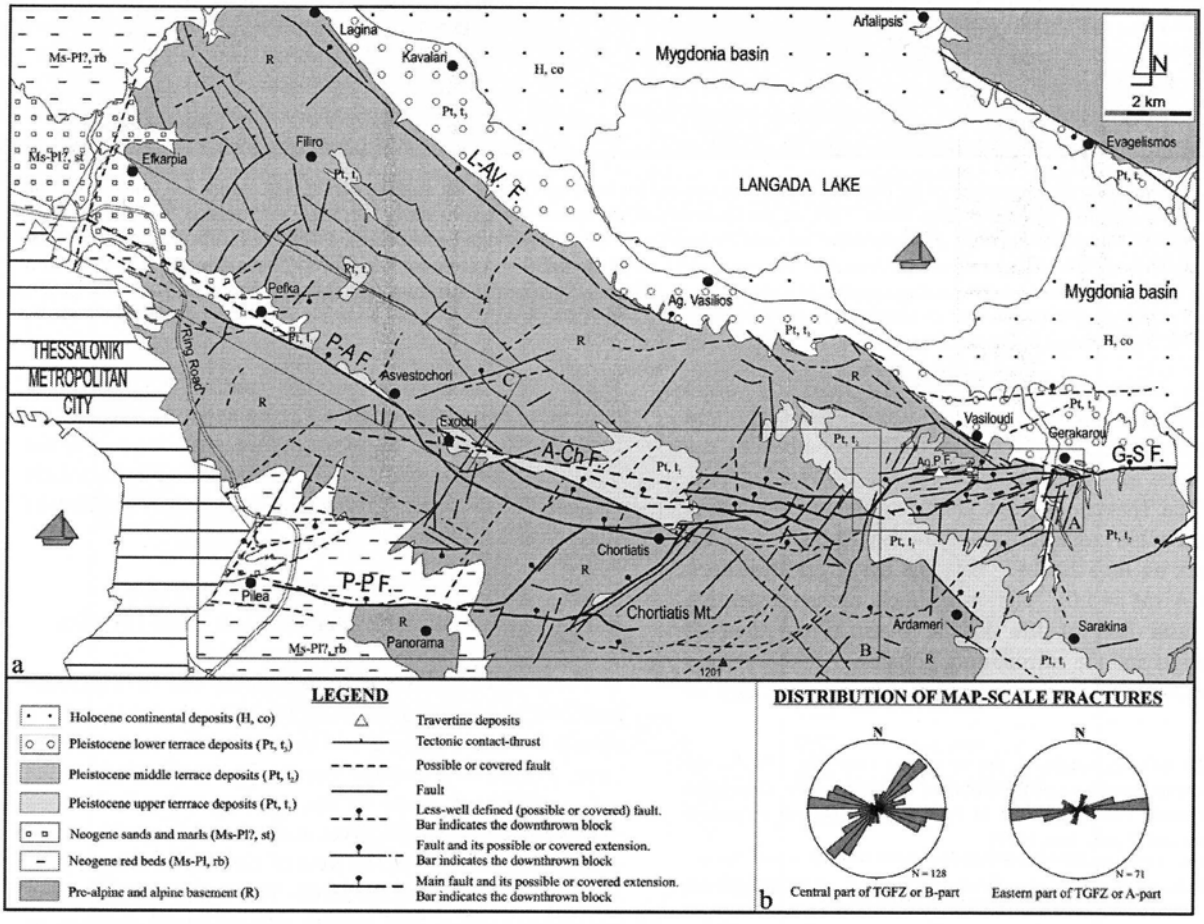

Fig. 3. (a) Geological-tectonic map of the mountainous area east of Thessaloniki showing the geometry of the TGFZ. Squares A, B, C are the eastern, central and western part of the TGFZ as described in the text. S–G F.: Stivos–Gerakarou Fault, Ag. P F.: Ag. Paraskevi Fault, A–Ch F.: Asvestochori–Chortiatis Fault, P–A F.: Pefka–Asvestochori Fault, P–P F.: Pilea–Panorama Fault, L–AV. F.: Lagina–Ag. Vasilios Fault. Thin lines with square tick marks are tectonic contacts. Thick lines, part broken, are the main fault traces of the TGFZ with solid bar tick marks pointing to the downthrown side of the faults. Thinner lines are the certain faults or the possible or covered faults (broken lines) mapped in the area. (b) Inset rose-diagram of the joints and faults in the eastern (A) and central (B) part of the TGFZ. Geological boundaries derived from the geological map at a scale of 1:50,000 of Thessaloniki (Kockel et al., 1978a) and Thermi (Kockel et al., 1978b).

western end of the Gerakarou–Stivos fault towards the Thessaloniki city, where the 1999 seismic sequence occurred.

For this purpose Landsat satellite images and air-photos at a scale of 1:33,000 were used. We propose that the Gerakarou–Stivos fault continues westwards through a large number of subparallel small fractures and large faults of E–W strike and N dip (Fig. 3a) up to Asvestochori village and the city of Thessaloniki forming a complicated fault zone named the Thessaloniki–Gerakarou Fault Zone (TGFZ).

3.1. Description of the TGFZ

In describing the TGFZ we subdivide it into three main parts: eastern (A), central (B) and western (C) (Fig. 3a). Different orientation and architecture as well as geologic features such as those that might be classified as 'barriers' or 'asperities', generally related to fault segmentation, characterize each part of the TGFZ. Among such features are minor fault bends (Bilham and Williams, 1985; King and Nabelek, 1985), en échelon stepovers (Bakum et al., 1980; Segall and Pollard, 1980; Deng and Zhang, 1984; Sibson, 1985), changing relief along the fault (Schwartz and Coppersmith, 1984; Crone et al., 1987), cross-structures (Schwartz and Coppersmith, 1986; Crone et al., 1987) and changing bedrock types and hydrologic environment (Allen, 1968; Irwin and Barnes, 1975).

3.1.1. Eastern part of the TGFZ

The eastern part of the TGFZ (A, in Fig. 3a) consists of the part, west and south of Gerakarou and Vasilloudi villages, respectively, where the well-defined Ardameri–Gerakarou sphenoid subbasin is exposed. This subbasin consists of part of the larger Pre-Mygdonia graben, the latter formed by the activation of the NW–SE-trending fault system from Middle Miocene to Pliocene (Psilovikos and Sotiriadis, 1983). The exposed sediments in the Ardameri–Gerakarou subbasin are red beds of Villafranchian (Lower Pleistocene) age that constitute the uppermost portion of the Pre-Mygdonia basin. They belong to the Gerakarou Formation and consist of alternating lens-shaped beds of unconsolidated gravels, coarse sands and reddish-brown silts and clays deposited in a fluvioterrestrial environment (Koufos et al., 1995). The Mygdonia graben has been developed along the Langada and Volvi lakes forming a narrow Quaternary sedimentary strip of NW–SE strike at the west and E–W strike at the east.

At this part, the TGFZ runs through the Ag. Paraskevi stream (Fig. 4a) forming the most prominent fault strand called Ag. Paraskevi fault. The eastern part of this fault, similar to the Gerakarou–Stivos fault, strikes ENE–WSW and dips to NNW, but to the west it bends towards a NNE–SSW orientation perpendicularly terminating at the more western Asvestochori–Chortiatis fault. Along this fault travertine deposits have been found. Hancock et al. (1999) suggested that many of the springs that are sources of travertine deposits are located in step-over zones between adjacent fault segments. Indeed, the same conditions have been found in this part of the TGFZ, where a 2.5-km-long extensional step-over zone between the left-stepping Gerakarou–Stivos fault and Asvestochori–Chortiatis fault is well established by our mapping.

Within this extensional step-over zone, fractures affecting the Pleistocene sediments of the Gerakarou Formation have been found, revealing a distinctly E–W strike with a mean value of N80° (eastern part or A, Fig. 3b). They comprise both joints and meso-scale extensional faults that drift the drainage pattern along their strike. Also, because of their presence, many subparallel NNE-drifted streams are captured more or less along the E–W lineaments. The observed joints are mostly vertical, single-layer fractures and are presented as non-continuous fractures with no uniform distribution, but their spacing on the scale of outcrop is relatively constant (Tranos and Mountrakis, 1998).

3.1.2. Central part of the TGFZ

In the central part (B, in Fig. 3a) of the TGFZ our mapping indicates that the fault pattern affecting the basement is dominated mostly by the WNW–ESE striking faults that dip to the N with high angles. NNE- to NE-trending faults dipping mostly to the WNW at high angles complete the fault pattern (central part or B, Fig. 3b). In detail, two main WNW–ESE-trending faults both dipping to the N constitute two subparallel major strands of the TGFZ at this part, the northern strand named Asvestochori–Chortiatis fault, trending 98°, and the southern named Pilea–Panorama fault, trending 99°. These faults are linked to each other, by two NNE- to NE-subparallel faults that both dip towards WNW.

The Asvestochori–Chortiatis fault is comprised of an array of subparallel, synthetic and successive in line fault strands dipping mainly to the N forming a crescent-shaped alignment at the large scale between the Asvestochori and Chortiatis villages. This fault stands at the westward prolongation of the Gerakarou–Stivos fault where it cuts the Chortiatis mountain chain, and where a NW–SE fabric dominates. However, some of the fault strands of the Asvestochori–Chortiatis fault pre-existed as thrust surfaces or surfaces of left-lateral thrust ramps of the CRBTS during the Tertiary (Tranos et al., 1999).

In particular, along the northern slopes of the Mt. Chortiatis and eastwards of the Chortiatis village, the Asvestochori–Chortiatis fault consists of at least three 100° striking subparallel synthetic fault strands dipping constantly towards the N at an angle of 60–80°. Among these strands, which gradually lower the northern slopes of the Mt. Chortiatis, the most prominent and rectilinear is the middle one reaching eastwards towards the Ag. Paraskevi fault. A prominent morphotectonic feature along these faults is the reversal of the relief due to the northward tilted

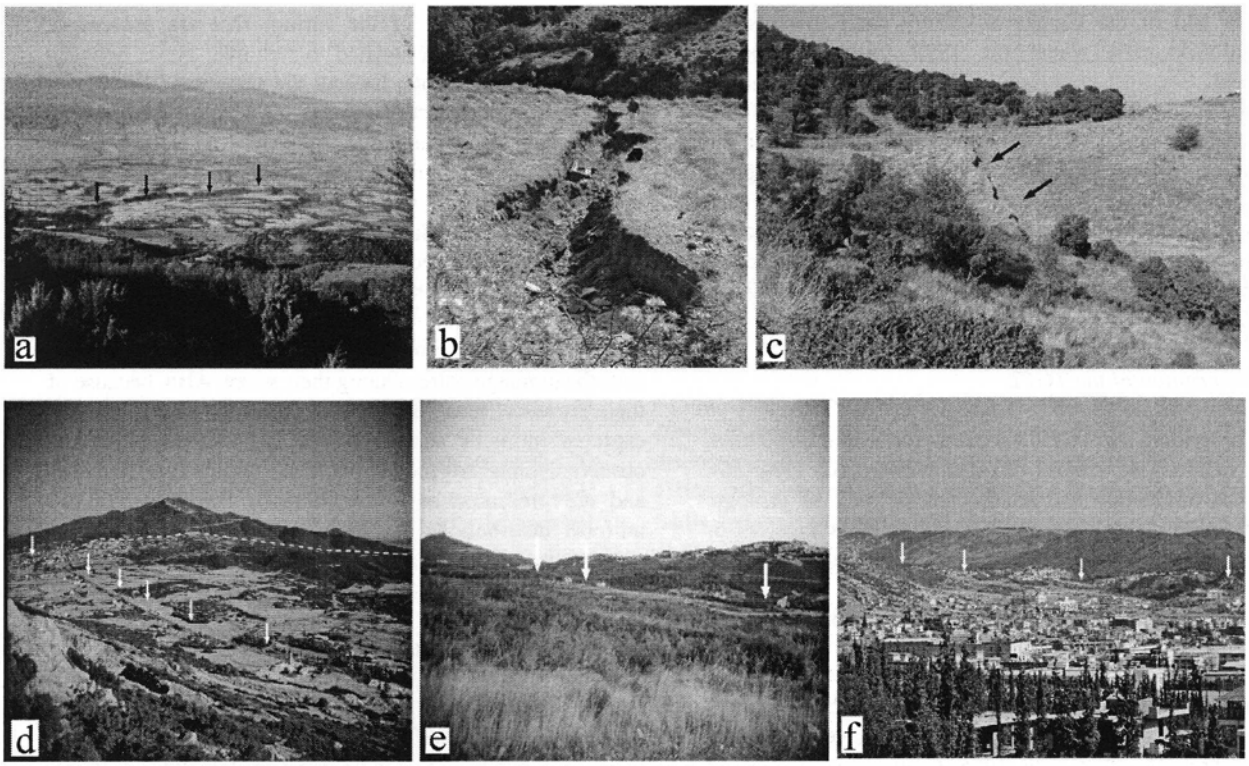

Fig. 4. Field photographs along the TGFZ showing the: (a) eastern part of the TGFZ. Solid arrows indicate the Ag. Paraskevi fault, (b) huge vertical fissure, possibly associated with the 1978 Thessaloniki main shock in the central part of the TGFZ (view towards E), (c) same as (b) but looking towards W, the fissure shown with black arrows, (d) central part of the TGFZ in the west part of Chortiatis village (view towards SE). White arrows indicate a strand of the Asvestochori–Chortiatis fault that bounds a small Quaternary valley to the south. In the background, the highest peak of Mt. Chortiatis is shown as well as the main NNE–SSW-trending fault (white broken lines) joining the Asvestochori–Chortiatis Fault with the Pilea–Panorama Fault, (e) Pilea–Panorama fault that forms a narrow rectilinear valley shown by white arrows, (f) western part of the TGFZ. The rectilinear alignment of the Pefka–Asvestochori fault is shown by the white arrows.

blocks. A vertical fissure striking 100° cuts the erosion mantle along the Northern Strand (Fig. 4b and c). This fissure has a length of about 50 m, a heave of 1.5 m and a depth of about 2–2.5 m, and is possibly associated with the 1978 main shock. Within this fissure, which appears fresh, one can observe a small brittle fault surface cutting the phylitic rocks underneath the erosion mantle at the base.

To the west, between the Asvestochori and Chortiatis villages, along the Asvestochori–Chortiatis fault, a valley filled to a depth of about 70 m (data from water wells) with Pleistocene fluvioterrestrial sediments (coarse sands and gravels) has developed. Although the valley obliterates the traces of the fault strands previously mentioned, it is delimited to the south by a southern fault strand of the Asvestochori–Chortiatis fault (Figs. 3a and 4d), thus suggesting that it is closely related to the Asvestochori–Chortiatis fault reactivation and could be characterised as a fault-bounded valley. In this part, more southern fault strands also belonging to the TGFZ have been mapped up to the Exochi and Asvestochori villages. They run through the northern part of the Chortiatis village and cut the NNE–SSW faults that depress Mt. Chortiatis to the west (Fig. 4d). In some localities, however, the NNE–SSW faults cut the major WNW–ESE faults. This reciprocal cutting between the WNW–ESE and NNE- to NE-trending faults suggests that both have simultaneously reactivated under a unique stress field.

The Pilea–Panorama fault strand, which is subparallel to the Asvestochori–Chortiatis fault, strikes WNW–ESE and dips to the N forming an elongated deep valley (Fig. 4e), filled with Neogene redbeds unconformably overlain by Quaternary sediments (Fig. 3a). The fault juxtaposes these sediments (hanging wall) against the ophiolitic rocks to the south (footwall). The fault has an observed length of about 8 km and possibly continues westwards to the Thessaloniki city cross-cutting a NNE–SSW fault. The Pilea–Panorama fault to the east joins successively to the NNE–SSW faults that rapidly lower the western slopes of Mt. Chortiatis, and links through them to the Asvestochori–Chortiatis fault. Therefore, in this intermountainous region the TGFZ bifurcates into two subparallel fault strands, the Asvestochori–Chortiatis and Pilea–Panorama, which, along with the NNE- to NE-faults, form at least two successive fault duplexes that dominate this part.

3.1.3. Western part of the TGFZ

Westwards of the Asvestochori village, the TGFZ continues through the 9.5-km-long Pefka–Asvestochori fault to the NW limits of Thessaloniki city where it possibly crosscuts a large NNE–SSW fault (C, Fig. 3a). The latter is considered as the western observed end of this segment of the TGFZ. Detailed tracing of the TGFZ on a Landsat image in between the Asvestochori and Exochi villages indicates that a minor fault bend exists between the Asvestochori–Chortiatis fault and the Pefka–Asvestochori fault. This minor fault bend is considered in this study as a distinctive barrier of the TGFZ because the latter exhibits a different orientation and architecture westwards of this point compared with the central part. The Pefka–Asvestochori fault passing through the Asvestochori and Pefka villages strikes WNW–ESE and forms a distinctly straight fault trace (Fig. 4f), along which a narrow valley partly filled with Neogene and Quaternary detrital sediments has been formed. E–W antithetic smaller faults in the hanging wall of the Pefka–Asvestochori fault dipping to the S at high angles complete the fault pattern in this western part. These faults control the hydrographic network of the valley, forming long parallel streams in an E–W orientation, and cutting small WNW–ESE faults that parallel the Pefka–Asvestochori fault.

Just after the 1978 earthquake, some 115° striking seismically-induced cracks were observed at the Polichni suburb (Papastamatiou, 1978; Mercier et al., 1983). Mercier et al. (1983) attributed these cracks to the Pefka–Asvestochori fault reactivation. Instead of finding similarly oriented cracks along this fault, we observe that an 80°-striking ground fissure of about 10 cm heave forms a hollow in the road running subparallel to the Pefka–Asvestochori fault (in its footwall). The fissure has been formed along an 80°-striking fault dipping at 84° to the N that affects the metaclastic rocks of the CRBTS, and it possibly indicates the tectonic instability of the area. It suggests that the least-principal stress axis (σ_3) is in the NNW–SSE (350°) orientation. This part of the TGFZ is characterized by low-intensity and high frequency seismicity. However, the calculated fault plane solutions could not define its geometry (Hatzidimitriou et al., 1991).

3.2. Kinematics

The kinematics of the TGFZ has been deduced using microstructures widely accepted as slip and sense-of-shear indicators such as slickenlines, accretion steps, Riedel structures and S–C cataclastic fabric (Hancock, 1985; Pettit, 1987). A significant problem arises from the fact that in Central Macedonia the faults affecting the basement rocks reveal a more complicated kinematics since their slickensides bear commonly more than one set of slickenlines (Pavlides and Kilias, 1987; Pavlides et al., 1990; Tranos, 1998; Tranos et al., 1999). To overcome this problem, we determined the chronological order of the different fault movements along the TGFZ by observations of cross-cutting structures, as well as superposition of the different sets of slickenlines and the associated cataclastic material. In addition, we correlate this chronological order with that derived from the faults and the fractures affecting the Neogene and mainly the Quaternary sediments, since the latter have been affected only by the N–S stress regime.

In the eastern part of the TGFZ the faults of the zone striking E–W cut mostly the Pleistocene sediments of the Gerakarou Formation. These faults bear only one set of slickenlines that indicate a normal to oblique left-lateral normal movement. Similarly orientated slickenlines indicating oblique left-lateral normal movement (rake: −60° to −90°) have also been observed along some faults affecting the exposed basement and along the Ag. Paraskevi fault (Fig. 5a). This fault movement fits well with the least principal stress axis (σ_3) determined by neotectonic joints affecting the Pleistocene sediments (Tranos and Mountrakis, 1998) and parallels the slip vector of the 1978 seismic fault defined by the focal solution of the main shock (Soufleris et al., 1982). In addition, these slickenlines are superposed on all the sets of slickenlines with different orientations and determine maximum extension from 355° to 27° (Tranos, 1998). Therefore, this fault displacement is the latest movement revealed by the E–W faults forming the TGFZ. The asymmetric rhomb-shape of the extensional duplex mapped at this part, which suggests a left-lateral component of the fault movement, fits well with this kinematics.

In the central part of the TGFZ, the WNW–ESE faults affecting the basement reveal at least three sets of slickenlines with different orientations indicating the following fault movements: (a) a left-lateral strike-slip movement, which is attributed to Oligocene–Miocene deformation (Tranos, 1998; Tranos et al., 1999), (b) an oblique right-lateral normal movement, which is attributed to the NE–SW extensional stress field of the Late Miocene–Pliocene times, and (c) an oblique left-lateral normal movement that is considered as the most recent. The WNW–ESE-trending Asvestochori–Chortiatis and Pilea–Panorama fault strands reveal oblique left-lateral normal to normal movement (rake: −60° to −90°) similar to the latest movement. This suggests strain compatibility between both these strands.

The kinematics of the NNE- to NE-trending faults is best defined along the faults cutting the carbonate rocks of the central part. These faults reveal at least three sets of slickenlines that define three different fault movements, which are from oldest to youngest: (1) left-lateral strike-slip movement (rake: 0–20° to 160–180°), (2) oblique left-lateral normal movement (rake: −60° to −80°), and (3) oblique right-lateral extensional movement (rake: −120° to −150°) as found by Tranos (1998). The latest one determines that the maximum extension strikes from 324° to 008° and reveals strain compatibility with the aforementioned normal to oblique left-lateral normal movement of

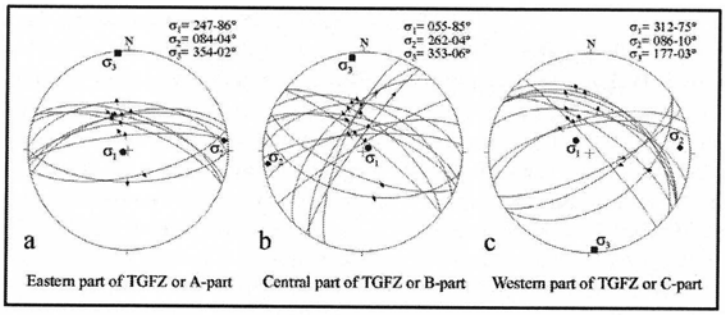

Fig. 5. Fault planes and slip vectors from the different parts of the TGFZ plotted on lower hemisphere equal-area stereonets. The paleostress axes are derived for each sub-area using the StereoNett software (Duyester, 1999). Square is the least principal stress axis (σ_3), rhomb is the intermediate principal stress axis (σ_2) and circle is the greatest principal stress axis (σ_1).

the WNW–ESE-trending faults (Fig. 5b). The recently recorded reactivation of these faults as indicated by focal mechanisms (Hatzidimitriou et al., 1991) supports their right-lateral oblique extensional movement and the simultaneous reactivation of the NNE- and WNW-trending faults. Finally, in the western part of the TGFZ, the oblique left-lateral normal movement is also the latest movement that characterizes the Pefka–Asvestochori fault and smaller antithetic E–W faults (Fig. 5c).

3.3. Seismotectonic implications of the TGFZ

Our investigation focusing on the fault geometry and kinematics suggests that the TGFZ could be the western extension of the 1978 earthquake fault. In particular, the E–W strike and the left-lateral oblique-normal movement of the TGFZ is similar to the geometry and kinematics of the 1978 earthquake fault as determined by the fault plane solution of the mainshock, the distribution of its aftershocks and the main active and seismic faults of the broader area of Chalkidiki and Central Macedonia (Mountrakis et al., 1983; Pavlides and Tranos, 1991; Tranos, 1998; Papazachos et al., 1998). Moreover, the isolated ground ruptures observed after the 1978 earthquake in the northern suburb of the Thessaloniki city and the occurrence of the latest 1999 seismic sequence in the central part of Mt. Chortiatis can be attributed to the reactivation of faults belonging to the TGFZ.

Papazachos et al. (2000) interpreted this latest 1999 seismicity to be caused by the reactivation of a NW–SE striking normal fault dipping to the SW under the city of Thessaloniki. However, there are some arguments concerning this interpretation. Our detailed mapping (Fig. 3) indicates that there is no significant normal fault striking NW–SE and dipping to the SW; there are only the main mapped faults of the TGFZ that strike WNW–ESE (100°) and dip towards the N. In addition, the NE–SW maximum extension defined by the focal mechanism does not fit well with the N–S maximum extension of the broader area determined by the latest kinematics of the faults (Pavlides and Kilias, 1987; Pavlides et al., 1990; Mountrakis et al., 1996; Tranos, 1998), the neotectonic joints (Tranos et al., 1995; Tranos and Mountrakis, 1998) and the focal mechanisms of the large earthquakes (Papazachos et al., 1998).

The A–A′ cross-section of the TGFZ, in the area from Panorama to the Mygdonia graben, relates the surficial geometry of the TGFZ to the spatial distribution of the 1999 sequence hypocenters (Fig. 6). It demonstrates that the N-dipping geometry of the TGFZ, as defined by the surficial mapping (Fig. 6a), is well verified by the spatial distribution of these hypocenters (Fig. 6b). More precisely, the TGFZ forms a ramp-flat geometry with both Pilea–Panorama and Asvestochori–Chortiatis fault strands dipping to the N at about 66–67° to a depth of 4 km, and it reaches northwards beneath the lakes to a depth of 13 km at 28°. Some events with focal depths around 13 km that occurred in the mountainous area beneath the Panorama–Chortiatis area possibly belong to the NNE (10°)-dipping Anthemountas Extensional Detachment Fault (AEDF), which reaches the Earth's surface south of Thessaloniki city and forms the 100° striking Anthemountas basin. The extensional detachment level thus seems to be around a depth of 12–13 km.

The geometrical and kinematical characteristics of the TGFZ and the spatial distribution of the seismic activity enrich our understanding of the general fault pattern of the study area. East of the Gerakarou–Stivos fault there are faults such as the Nea Apollonia, Kokalou–Nea Madytos and Rendina that form almost identical geometries to that of the TGFZ and Gerakarou–Stivos fault (Fig. 7). They are characterised by similar kinematics to the TGFZ and Stivos–Gerakarou faults (Mountrakis et al., 1994, 1996) and more travertine deposits analogous to that of the eastern part of the TGFZ have been found along them. The fact that these travertine deposits have been superimposed on top of the Middle–Late Pleistocene sediments of the Mygdonian system (Sotiriadis et al., 1972; Psilovikos and Sotiriadis, 1983) strongly suggests the Quaternary reactivation of these faults. Therefore, it is suggested that both the 1978 earthquake fault and the TGFZ belong to a 65-km-long E–W-trending rupture fault system that extends from the Strymonikos gulf to the east, through the southern part of

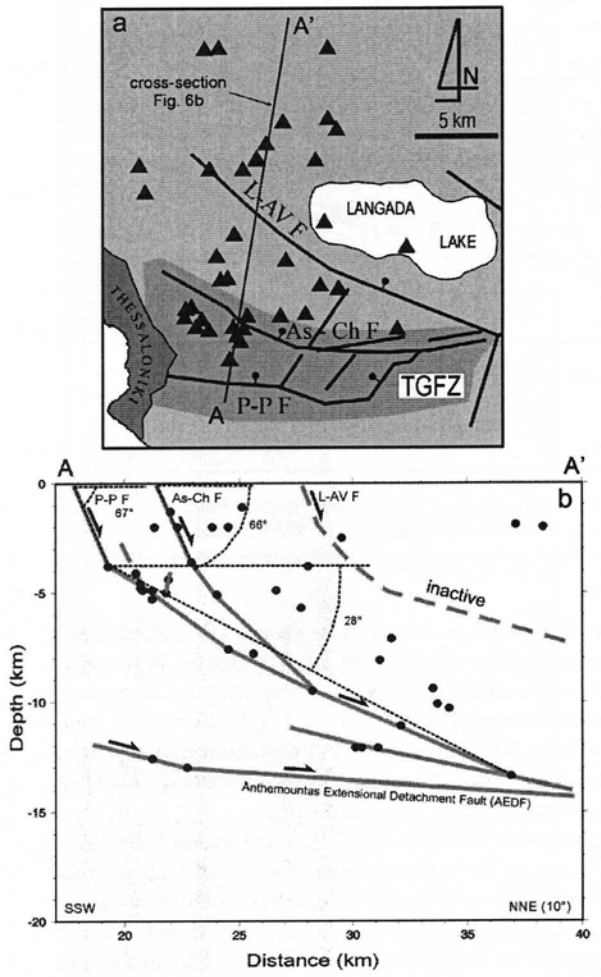

Fig. 6. (a) Part of the map of Fig. 2 showing the TGFZ geometry in the mountainous area east of Thessaloniki where the 1999 earthquake sequence occurred (triangles are the epicentres of the 1999 sequence). A–A′ is the cross-section in (b). (b) Cross-section in NNE–SSW orientation showing the distribution of the hypocentres in combination with the geometry of the Pilea–Panorama fault (P–P F.), Asvestochori–Chortiatis Fault (A–Ch F.) and Lagina–Ag. Vasilios Fault (L–AV F.). The Anthemountas Extensional Detachment Fault (AEDF) has been drawn taking also into account its fault trace and geometry. The dip-angle of the P–P F. and the As–Ch F. are indicated in respect to the depth. The trace of the cross-section is shown in Fig. 2 and (a).

the Mygdonia graben, to the city of Thessaloniki at the west. This fault system, here called Thessaloniki–Rentina Fault System (TRFS) (Fig. 7) consists of 17–20-km-long left-stepping 100°-trending main fault strands that form underlapping steps bridged by 8–10-km-long ENE–WSW faults so that the general trend of the TRFS is orthogonal to the regional active N–S extension stress field. This specific fault geometry of the TRFS has been clearly verified in the area of Stivos by the 1978 seismic sequence. In particular, the foreshock that occurred on 23 May 1978 with $M_s = 5.8$ has a fault plane solution indicating a 85° fault plane that is associated on the surface with similarly oriented seismic ground ruptures along the Gerakarou–Stivos fault, whereas the main shock occurred on 20 June 1978, has a fault plane solution that indicates a 100° fault plane and distribution of aftershocks along the same orientation. Thus the ENE–WSW Gerakarou–Stivos fault is considered as the bridge fault joining the Nea Apollonia fault (Mountrakis et al., 1996) at the east with the TGFZ.

In order to estimate the slip-rate of the TRFS, we take into account the maximum downthrow of the Lower Pleistocene/Middle Pleistocene contact between the sediments of the Pre-Mygdonia and Mygdonia groups. This contact coincides with the uppermost surface of the Gerakarou Fm., and its downthrow due to the TGFZ and Gerakarou–Stivos fault segments of the TRFS as estimated from drilling data, (BRGM and YEV drillings, in Psilovikos, 1977) is about 350 m. Therefore the slip-rate of the TRFS is very small, approximately 0.4 mm/y. As a result, the Mygdonia graben, which is fault-bounded to the TRFS at the south, is not as deep as would be expected from the intense seismicity of the area. Comparably shallow depths characterise most Quaternary sediments in the fault-bounded basins established along the CRBTS and the Serbomacedonian massif (Kockel et al., 1977; Mountrakis et al., 1983; Syrides, 1990). Although this contradiction needs further research, we think that the small slip-rate determined by these Quaternary sediments can be explained by the strain diffusion through the reactivation of the many N100°-trending faults that already existed within the general fault pattern, and the fact that they possibly have large periods of reactivation. There are a large number of 15–20-km-long active 100° striking faults dispersed throughout the Chalkidiki peninsula and the Central Macedonia, as well as similarly dispersed seismicity including earthquakes with magnitudes in the range 5.5–6.5.

The TRFS reveals different morphotectonic features along its length, which depict the different slip rates along its segments. In the area between Gerakarou and Nea Madytos villages, where the Gerakarou–Stivos, Nea Apollonia and Kokalou–Nea Madytos faults exist, it causes a strong imprint or modification of the pre-existing NW–SE fabric. On the other hand, in the mountainous area of Thessaloniki the pre-existing NW–SE fabric is significantly less modified by the TGFZ, which is characterised by tree-like fault geometry towards the city of Thessaloniki, comprising of 100°-trending faults that, along with the NNE- to NE-faults, form multi-level branching. Therefore, the TGFZ seems to reveal a rather 'embryonic' development in that mountainous area both in horizontal and vertical directions with the strain distributed along several inherited faults, possibly joined by small neo-formed faults.

4. Stress changes and triggering of seismicity during the 1978 seismic sequence

The geometry of the TRFS at the part of the 1978 seismic rupture as described previously, along with the fact that the

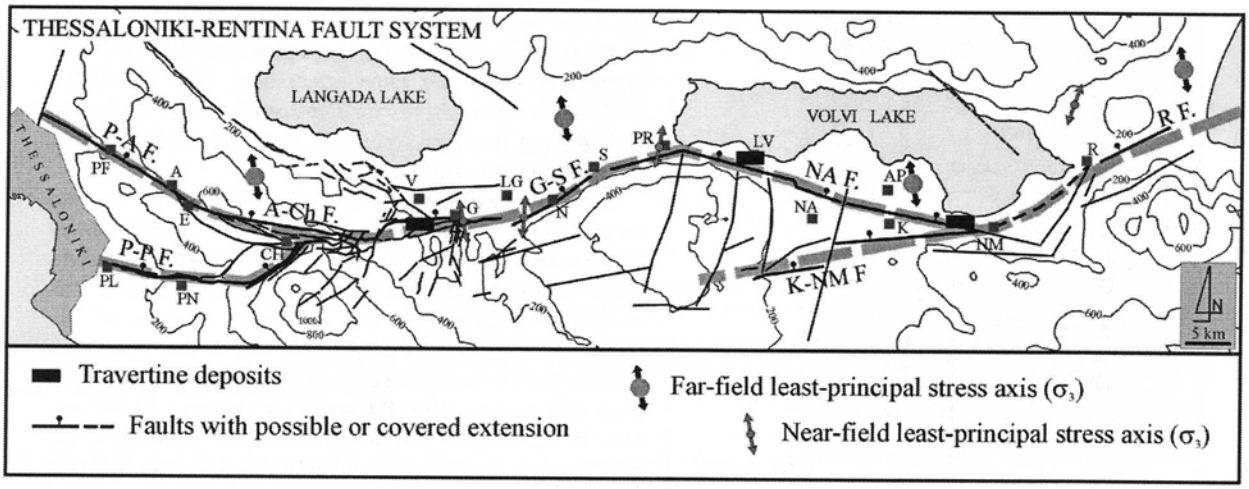

Fig. 7. General map of the Thessaloniki–Rentina Fault System (TRFS) with its several fault segments: P–A F.: Pefka–Asvestochori Fault, P–P F.: Pilea–Panorama Fault, A–Ch F.: Asvestochori–Chortiatis Fault, G–S F.: Gerakarou–Stivos Fault, NA F.: Nea Apollonia Fault, K–NM F.: Kokalou–Nea Madytos Fault, R F.: Rentina Fault. Villages indicated as in Fig. 2. Near-stress field orientations from Tranos and Mountrakis (1998) and far-stress field orientations from Papazachos and Kiratzi (1996) and Tranos (1998).

1978 earthquake sequence has been separated temporarily and spatially into two main sub-sequences (May 8–June 1 and June 1–July 2; after Papazachos et al., 1982) corresponding to foreshock (eastern part) and mainshock (western part), led us to suggest that the 1978 seismic rupture occurred initially along the ENE–WSW Gerakarou–Stivos fault, whereas the mainshock took place later along the WNW–ESE-trending TGFZ (Fig. 8). Moreover, the limit of aftershock activity of the 1978 mainshock seems to coincide well with the distinctive barrier of the TGFZ in between the Asvestochori–Chortiatis fault and the Pefka–Asvestochori fault. The migration of seismic activity from the Stivos–Gerakarou fault to the TGFZ (faults which are characterised by small strike difference), suggests that the latter was reacting to changes in the stress transfer induced by movement along the former. Slip on a section of an en échelon fault segment would change the surrounding stress field and therefore could affect the location of the next fault segment to experience slip. Therefore, it is of importance to investigate possible triggering in the study area.

Stress changes, i.e., values of ΔCFF (changes in Coulomb failure function), caused by the May 23, 1978 (M = 5.8) earthquake are computed for a dip-slip fault, specifically for the fault determined for the June 20, 1978 (M = 6.5) main shock. The stress calculations are performed for an isotropic elastic half space (Erikson, 1986; Okada, 1992). The shear modulus and Poisson's ratio are fixed as 33 GPa and 0.25, respectively. The value of the apparent coefficient of friction, μ', is taken equal to 0.4 in the calculations of this study, considering previous relative research. Extensive discussions on the choice of this value have been made by Deng and Sykes (1997a,b), who have taken μ' equal to 0.2 or 0.6 in their computations and found that the results are not very sensitive to the changes of this parameter. The stress field was computed at a depth of 10 km. This depth is chosen to be several kilometres above the bottom of the seismogenic layer, which in this case is considered to be about 15 km, as derived from aftershock hypocentral determination. This is in agreement with King et al. (1994), who found seismic slip peaks at mid-depths in the seismogenic zone, and thus deformation must be localized on the faults at these depths.

Furthermore, the fault length (L) and average displacement (u) must be known, since these are two parameters necessary for the model application. The distribution of the slip is actually non-uniform along a fault, but we are interested in its average value, as well as for a fault length expressing the main rupture. To a first approximation, scaling laws derived for a certain area can be used for the estimation of these parameters. For this reason, we used the following scaling laws suggested by Papazachos (1989) for the broader area of Greece, in order to calculate both these values, as a function of the magnitude, M, of the particular earthquake:

$$\log L = 0.51M - 1.85 \quad (1)$$

$$\log u = 0.82M - 3.71 \quad (2)$$

Using the scaling laws of Eqs. (1) and (2), a fault length equal to 13 km and a slip equal to 11 cm have been estimated for the May 23 event. Taking into account the total length of the ground ruptures associated with this event aligned along the Gerakarou–Stivos fault and the aftershock distribution during the period May 8–June 1 (Fig. 8a and b), a fault length equal to 10 km has been adopted in our model. The rupture model is approximated by rectangular surface, dipping at 46°, with two edges parallel to the Earth's surface. Although the rupture is more complicated and

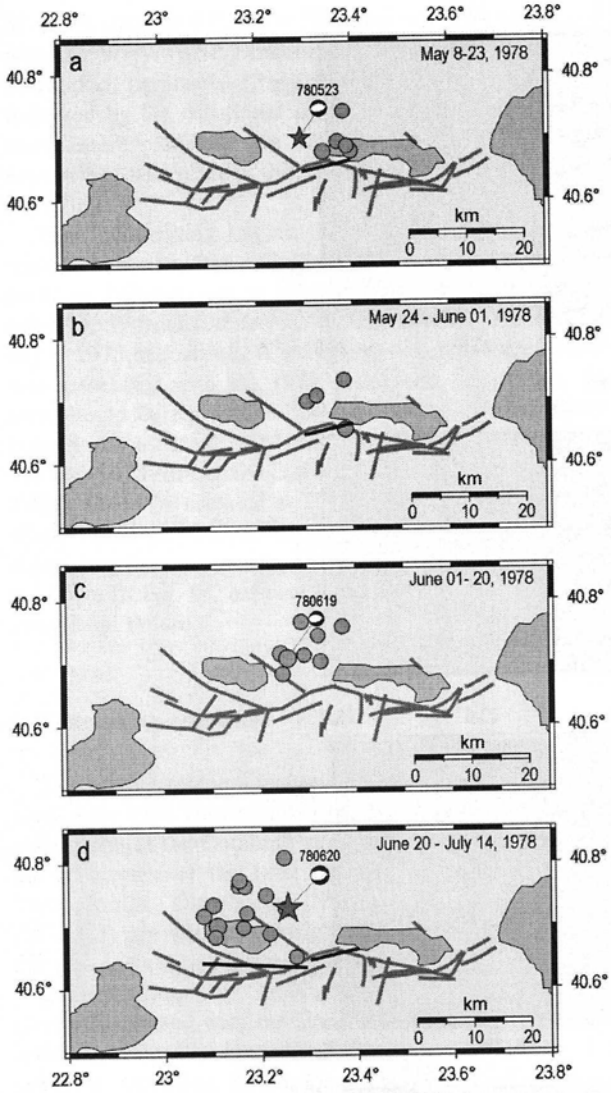

Fig. 8. Epicentral distribution of the events of the 1978 seismic sequence with M ≧ 4.3 that occurred during: (a) May 8–23, (b) May 24–June 1, (c) June 01–June 20, 1978, (d) June 20–July 14 (after Papazachos et al., 1982). Fault plane solutions of the larger events are presented as lower hemisphere equal area projections. Fault traces (grey lines) and the estimated rupture lengths of the May 23 and June 20 earthquakes are shown by heavy lines.

displacement varies along its segments, it is believed that the above approximation is sufficient to identify areas of enhanced future activity by stress changes caused by the main event.

The co-seismic stress changes associated with the May 23 strong shock are computed and shown in Fig. 9a. The technique applied here enables the inversion of the computed stress field according to the fault plane solution of the earthquake whose triggering is inspected. Therefore, the stress field is computed for a dip-slip fault striking 278° and dipping at 46° to the N, according to the fault plane solution of the main event (June 20, 1978), which is representative for the study area. In Fig. 9a, dark regions denote negative changes in Coulomb stress and decreased likelihood of fault rupture. These regions are called stress shadows following the terminology of Harris and Simpson (1993, 1996). Light regions represent positive ΔCFF and increased likelihood of rupture. The positive regions are called stress bright zones. It should be noted here that since stress is a tensorial and not a scalar quantity, shadow and bright zones must be viewed in the context of specified styles of fault slip, i.e. similar strike, dip, and rake (Deng and Sykes, 1997a). For example, a particular location could be situated in a bright zone for strike-slip faults, while it could be located in a shadow zone for thrust faults. In this figure faults are also projected at a depth of 10 km. The May 23 event created bright zones located along the main fault zone both to the west and east of its rupture. The main shock (M = 6.5) occurred in the region where positive changes in Coulomb failure function (ΔCFF) had the largest values. This shows that the May 23 shock enhanced stress and brought the adjacent fault segment closer to failure.

The ΔCFF was also computed on a plane dipping at 46° to the N and having a strike of 278°, that is, for a plane containing the fault plane of the June 20 main shock. Stress changes are shown in Fig. 9b along with the hypocentres of the three largest events of the sequence, projected onto the computation plane. It is evident that the main shock occurred in an area where positive ΔCFF had the largest values. The above demonstrates that the location and geometry of these largest earthquakes agree well with the pattern of Coulomb stress changes, suggesting elastic interaction between the different fault segments.

The cumulative ΔCFF, just after the main shock, is shown in Fig. 9c. The length of the causative fault for the June 20 mainshock is considered equal to 20 km, according to the spatial distribution of its aftershocks (Fig. 2), the geometry of the TGFZ is as defined in the present paper, and the location of a barrier is identified with the limit of aftershock activity (Fig. 8d), being in quite good agreement with a value of 25 km resulting from Eq. (1). The strike provided by the fault plane solution is in excellent agreement with the strike found by the structural analysis of the TGFZ described in the previous paragraph. The location of all aftershocks to the north of the fault trace supports the northward dip of the TGFZ.

Since our main concern is the possible continuation of the seismic activity to the west of the rupture zone of the 1978 main shock, we compute the stress field at a depth of 8 km and according to the geometry of the TGFZ, which is dominated by the N100° strike. Bright zones are created to the east and west of the causative fault as expected for normal faults, showing the areas where failure is expected in the future. It appears that the TGFZ and the Nea Apollonia fault (Mountrakis et al., 1996), projected in Fig. 9c, are brought closer to failure at the computation depth by enhanced stress after the occurrence of the June mainshock. The Nea Apollonia fault, however, has moved away from failure by the large Ierissos earthquake (26 September 1932,

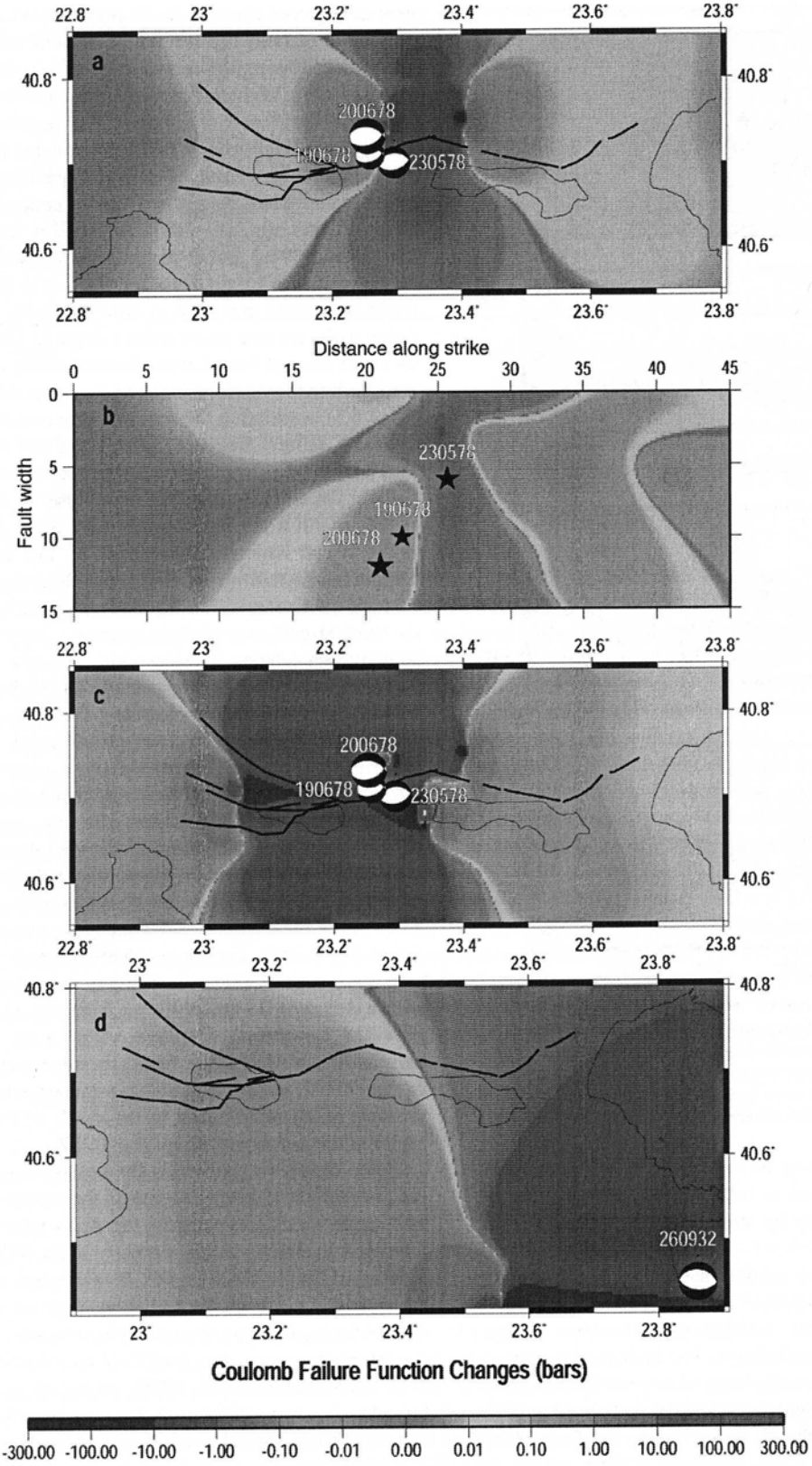

M = 7.0, strike = 93°, dip = 53°, rake = −93°) associated with the WNW–ESE Stratoni fault in the SE part of the Chalkidiki peninsula (Pavlides and Tranos, 1991) as indicated by the calculated ΔCFF (Fig. 9d). Therefore, it seems more plausible that the future seismic activity is expected to take place at the western part of the TRFS, i.e. the TGFZ.

The 130°-striking Lagina–Ag. Vasilios fault does not seem to be the western prolongation of the 1978 earthquake fault, as believed up to now, because its strike differs significantly from that derived from the fault plane solution of the 1978 mainshock. If we accept that this fault branch was associated with the 1978 mainshock occurrence, its rake should be equal to −35° (i.e. strike-slip movement) instead of the actual −70°, to be dynamically compatible with the 1978 earthquake fault so that an almost horizontal T-axis would be oriented at 17°, as derived from the fault plane solution. Additionally, Coulomb stress changes induced by the mainshock of the 1978 earthquake sequence as shown in Fig. 9c, indicate that this fault branch moved away from failure.

5. Concluding remarks

The present research including fault mapping in the area west of the 1978 Thessaloniki earthquake fault as well as the elaboration of the Coulomb stress changes associated with the occurrence of the 1932 Ierissos (M = 7.0) and 1978 Thessaloniki foreshock (M = 5.7) and mainshock (M = 6.5) provides new insights to the active faulting of the area and seismic hazard assessment.

In particular, the Gerakarou–Stivos fault, which is clearly associated with the latest destructive 1978 Thessaloniki earthquake sequence, continues westwards to the presently described 20-km-long Thessaloniki–Gerakarou Fault Zone (TGFZ) and does not continue to the NW–SE-trending Lagina–Ag. Vasilios fault as previously considered. The TGFZ reaches the city of Thessaloniki and it is compatible with the contemporary regional N–S extensional stress field that tends to modify the pre-existed NW–SE tectonic fabric that dominates the mountainous region of Thessaloniki.

Both the Gerakarou–Stivos fault and TGFZ belong to a ca. 65-km-long E–W-trending fault system, the Thessaloniki–Rendina Fault System (TRFS), that extends from the Strymonikos gulf to the east to the city of Thessaloniki to the west running through the southern part of the Mygdonian graben. This fault system consists of two 17–20-km-long left-stepping 100°-trending main fault strands that form underlapping steps bridged by 8–10-km-long ENE–WSW faults. The TRFS reveals different morphotectonic features along its length, which represent the different slip rate along its segments. In the area east of Gerakarou village, where it consists of the Gerakarou–Stivos, Nea Apollonia and Kokalou–Nea Madytos faults, it causes a strong imprint or modification of the older NW–SE fabric. In the mountainous area of Thessaloniki, where the TGFZ has been recognised, the modification of the NW–SE fabric is significantly less. As a result, the TGFZ reveals a rather 'embryonic' development in both horizontal and vertical directions with the strain distributed along several inherited faults, possibly joined by small neo-formed faults.

Historical information and instrumental data demonstrate that the whole TRFS has repeatedly experienced strong (M > 6.0) earthquakes. However, the continuation of this activity towards the west resulted from Coulomb stress changes associated with the 1932 and 1978 events. Therefore, the possible reactivation of the TGFZ, which constitutes the westernmost segment of the TRFS, represents a major threat for the city of Thessaloniki that has already experienced the destructive consequences of the 1759 earthquake.

The results obtained in this study indicate that tectonic analysis in combination with the Coulomb stress changes can be a valuable exploratory tool as well as a device for investigating well-established fault systems and to make implications on the future seismic hazard assessment of rupture zones.

Acknowledgements

We are grateful to Demosthenis Mountrakis for his careful and constructive review. We also thank C. Vita Finzi and an anonymous reviewer for their insightful reviews and comments that enabled us to improve upon our original manuscript. Editorial assistance by Tom Blenkinsop is greatly appreciated. We also thank Vagelis Kakouros and Deborah Ireland-Low for their linguistic comments on the manuscript. The first author thanks Andreas Elias for his assistance on taking photos of the paper. We also express thanks to C. Papazachos for providing us the original seismological information of the 1999 earthquake sequence. Stress tensors were calculated using a program written by J. Deng (Deng and Sykes, 1997a) who used the DIS3D code of S. Dunbar and Erikson (1986) and the expressions of G. Converse. The GMT system (Wessel and Smith, 1995)

Fig. 9. Changes in the Coulomb failure function (ΔCCF) associated with the occurrence of the largest events in the study area. The stress pattern is calculated for normal faulting. Changes are denoted by greyscale at the bottom (in bars). Fault plane solutions are plotted as lower-hemisphere equal area projections. The date (d/m/y) of each event is given on top of the projections. (a) Co-seismic Coulomb stress changes associated with the May 23 event. (b) Coulomb stress changes after May 23 event calculated onto the fault plane of the June 20 event. (c) State of stress after the occurrence of the June 20 main shock. (d) Co-seismic Coulomb stress changes associated with the September 26, 1932 earthquake.

was used to plot some of the figures. Department of Geophysics Contribution 605. This paper is partly supported by project 20441 funded by the Region of Central Macedonia (Greece) and projects 20237 and 20321 funded by Earthquake Planning and Protection Organization (Greece).

References

Allen, C.R., 1968. The tectonic environments of seismically active and inactive areas along the San Andreas fault system. Stanford University Publications in the Geological Sciences 11, 70–82.

Angelier, J., 1979. Neotectonique de l' Arc Egeen. Ph.D. Thesis, University Paris VI, in French.

Bakum, W.H., Stewart, R.M., Bufe, C.G., Marks, S.M., 1980. Implication of seismicity for failure of a section of the San Andreas rift. Bulletin of the Seismological Society of America 70, 185–201.

Bilham, R., Williams, P., 1985. Sawtooth segmentation and deformation processes on the southern San Andreas fault, California. Geophysical Research Letters 12, 557–560.

Carver, D., Bollinger, G.A., 1981. Aftershocks of the June 20, 1978, Greece earthquake: a multimode faulting sequence. Tectonophysics 73, 343–363.

Chatzipetros, A.A., Pavlides, S.B., 1998. A quantitative morphotectonic approach to the study of active faults; Mygdonia basin, Northern Greece. Bulletin of Geological Society of Greece 32, 155–164.

Crone, A.J., Machette, M.N., Bonilla, M.G., Lienkaemper, J.J., Pierce, K.L., Scott, W.E., Bucknam, R.C., 1987. Surface faulting accompanying the Borah Peak earthquake and segmentation of the Lost River fault, central Idaho. Bulletin of the Seismological Society of. America 77, 739–770.

Deng, J., Sykes, L.R., 1997a. Evolution of the stress field in southern California and triggering of moderate-size earthquakes: a 200-year perspective. Journal of Geophysical Research 102, 9859–9886.

Deng, J., Sykes, L.R., 1997b. Stress evolution in southern California and triggering of moderate-, small-, and micro-size earthquakes. Journal of Geophysical Research 102, 411–435.

Deng, Q., Zhang, P., 1984. Research on the geometry of shear fracture zones. Journal of Geophysical Research 89, 5699–5710.

Duyester, J.D., 1999. StereoNett, vers. 2.4, http://homepage.ruhr-uni-bochum.de/Johannes.P.Duyester/Stereo/Stereo1.htm.

Erikson, L., 1986. User's manual for DIS3D: a three-dimensional dislocation program with applications to faulting in the Earth. M.Sc. Thesis, Stanford University.

Hancock, P.L., 1985. Brittle microtectonics: principles and practice. Journal of Structural Geology 7, 437–457.

Hancock, P.L., Chalmers, R.M.L., Altunel, E., Cakir, Z., 1999. Travitonics: using travertines in active fault studies. Journal of Structural Geology 21, 903–916.

Harris, R.A., Simpson, R.W., 1993. In the shadow of 1857, an evaluation of the stress changes generated by the M8 Ft. Tejon, California, earthquake (abstract). Eos Transaction AGU, 74(43), Fall Meeting Supplementary, p. 427.

Harris, R.A., Simpson, R.W., 1996. In the shadow of 1857—the effect of the great Ft. Tejon earthquake on the subsequent earthquakes in southern California. Geophysical Research Letters 23, 229–232.

Hatzfeld, D., Christodoulou, A.A., Scordilis, E.M., Panagiotopoulos, D., Hatzidimitriou, P.M., 1987. A microearthquake study of the Mygdonian graben (northern Greece). Earth and Planetary Science Letters 81, 379–396.

Hatzidimitriou, P.M., Scordilis, E.M., Papadimitriou, E.E., Hatzfeld, D., Christodoulou, A.A., 1991. Microearthquake study of the Thessaloniki area (northern Greece). Terra Nova 3, 648–654.

Hubert-Ferrari, A., Barka, A., Jacques, E., Nalbant, S.S., Meyer, B., Armijo, R., Tapponnier, P., King, G.C.P., 2000. Seismic hazard in the Marmara sea region following the 17 August 1999 Izmit earthquake. Nature 404, 269–273.

Irwin, W.P., Barnes, I., 1975. Effects of geological structure and metamorphic fluids on seismic behaviour of the San Andreas fault system in central and northern California. Geology 3, 713–716.

King, G.C.P., Nabelek, J., 1985. Role of fault bends in the initiation and termination of earthquake rupture. Science 228, 984–987.

King, G.C.P., Stein, R.S., Lin, J., 1994. Static stress changes and the triggering of earthquakes. Bulletin of the Seismological Society of America 84, 935–953.

Kockel, F., Mollat, H., Walther, H.W., 1977. Erlauterungen zur Geologischen Karte der Chalkidiki und angrenzender Gebiete 1:100,000 (Nord-Griechenland). Bundesanstalt fur Geowisseschaften und Rohstoffe, Hannover, 119pp.

Kockel, F., Antoniadis, P., Ioannidis, K., 1978a. Geological map of Greece, Thessaloniki sheet. Institute of Geology and Mineral Exploration of Greece, scale 1:50,000.

Kockel, F., Mollat, H., Antoniadis, P., Papadopoulos, P., 1978b. Geological map of Greece, Thermi sheet. Institute of Geology and Mineral Exploration of Greece, scale 1:50,000.

Koufos, G.D., Syrides, G.E., Kostopoulos, D.S., Koliadimou, K.K., 1995. Preliminary results about the stratigraphy and palaeoenvironment of Mygdonia basin, Macedonia, Greece. Geobios 18, 243–249.

Mercier, J.-L., 1981. Extensional–compressional tectonics associated with the Aegean arc: comparison with the Andean Cordillera of south Peru–north Bolivia. Philosophical Transactions of the Royal Society of London A 300, 337–355.

Mercier, J.-L., Carey-Gailhardis, E., Mouyaris, N., Simeakis, K., Roundoyannis, Th., Anghelidhis, Ch., 1983. Structural analysis of recent and active faults and regional state of stress in the epicentral area of the 1978 Thessaloniki earthquakes (Northern Greece). Tectonics 2, 577–600.

Mercier, J.-L., Simeakis, K., Sorel, D., Vergely, P., 1989. Extensional tectonic regimes in the Aegean basins during the Cenozoic. Basin Research 2, 49–71.

Mountrakis, D., Psilovikos, A., Papazachos, B.C., 1983. The geotectonic regime of the Thessaloniki earthquakes. In: Papazachos, B.C., Carydis, P.G. (Eds.), The Thessaloniki, Northern Greece, Earthquake of June 20, 1978 and Its Seismic Sequence, Technical Chamber of Greece, pp. 11–27.

Mountrakis, D., Kilias, A., Pavlides, S., Psilovikos, A., Vavliakis, E., Syrides, G., Scordilis, M., Tranos, M., Spyropoulos, N., Zouros, N., Fasoulas, Ch., 1994. Kinematics and dynamics of the neotectonic deformation in the area of Volvi-Eastern Chalkidiki. Edition of the neotectonic map, sheet Rhodolivos, Earthquake Planning and Protection Organisation.

Mountrakis, D., Kilias, A., Pavlides, S., Sotiriadis, L., Psilovikos, A., Astaras, Th., Vavliakis, E., Koufos, G., Dimopoulos, G., Soulios, G., Christaras, V., Skordilis, M., Tranos, M., Spyropoulos, N., Patras, D., Syrides, G., Lambrinos, N., Laggalis, T., 1996. Neotectonic map of Greece, Langadhas sheet. Earthquake Planning and Protection Organisation and European Center on Prevention and Forecasting of Earthquakes, scale 1:100,000.

Okada, Y., 1992. Internal deformation due to shear and tensile faults in a half-space. Bulletin of the Seismological Society of America 82, 1018–1040.

Papadimitriou, E.E., Karakostas, V.G., Papazachos, C.B., 2001. Rupture zones in the area of the 17.08.99 Izmit (NW Turkey) large earthquake (M_w7.4) and stress changes caused by its generation. Journal of Seismology 5, 269–276.

Papastamatiou, D.J., 1978. The 1978 Chalkidiki earthquakes in N. Greece, a preliminary field report and discussion. Technical note, Dames and Moore, TN-LN-28, London.

Papazachos, B.C., 1989. Measures of earthquake size in Greece and surrounding areas. Proceedings of the 1st Scientific Conference of

Geophysics. Geophysical Society of Greece, April 19–21, 1989, Athens, pp. 438–447.

Papazachos, B.C., Papazachou, C., 1997. The Earthquakes of Greece, Ziti Publications, Thessaloniki.

Papazachos, B.C., Mountrakis, D., Psilovikos, A., Leventakis, G., 1979. Surface fault traces and fault plane solutions of May–June 1978 major shocks in the Thessaloniki area. Tectonophysics 53, 171–183.

Papazachos, B.C., Tsapanos, T.M., Panagiotopoulos, D.G., 1982. A premonitory pattern of earthquakes in northern Greece. Nature 296, 232–235.

Papazachos, B.C., Papadimitriou, E.E., Kiratzi, A.A., Papazachos, C.B., Louvari, E.K., 1998. Fault plane solutions in the Aegean and the surrounding area and their tectonic implications. Bolletino Geofisica Teorica Applicata 39, 199–218.

Papazachos, C.B., Kiratzi, A.A., 1996. A detailed study of the active crustal deformation in the Aegean and surrounding area. Tectonophysics 253, 129–153.

Papazachos, C.B., Soupios, P., Savvaidis, A., Roumelioti, Z., 2000. Identification of small-scale active faults near metropolitan areas: an example from the Asvestochori fault near Thessaloniki, Proceedings of the XXXII ESC General Assembly, Lisbon, Portugal, 15–20 September 2000, pp. 221–225.

Parsons, T., Toda, S., Stein, R.S., Barka, A., Dieterich, J.H., 2000. Heightened odds of large earthquakes near Istanbul: an interaction-based probability calculation. Science 288, 661–665.

Pavlides, S.B., 1993. Active faulting in multi-fractured seismogenic areas; examples from Greece. Zeitschrift für Geomorphologie 94, 57–72.

Pavlides, S.B., Kilias, A.A., 1987. Neotectonic and active faults along the Serbomacedonian zone (Chalkidiki, N. Greece). Annales Tectonicae 1, 97–104.

Pavlides, S.B., Tranos, M.D., 1991. Structural characteristics of two strong earthquakes in the North Aegean: Ierissos (1932) and Agios Efstratios (1968). Journal of Structural Geology 13, 205–214.

Pavlides, S., Mountrakis, D., Kilias, A., Tranos, M., 1990. The role of strike-slip movements in the extensional area of the northern Aegean (Greece). In: Boccaletti, M., Nur, A. (Eds.), Active and Recent Strike-slip Tectonics. Annales Tectonicae 4, pp. 196–211.

Pettit, J.P., 1987. Criteria for the sense of movement on fault surfaces in brittle rocks. Journal of Structural Geology 9, 597–608.

Psilovikos, A., 1977. Paleogeographic development of the basin and lake of Mygdonia (Langada-Volvi area, Greece), Ph.D. Thesis, Univ. Thessaloniki, in Greek.

Psilovikos, A., Sotiriadis, L., 1983. The neotectonic graben complex of the Serbomacedonian massif at the area of Premygdonian basin, in northern Greece. Clausthaler Geologische Abhandlungen 44, 21–52.

Schwartz, D.P., Coppersmith, K.J., 1984. Fault behaviour and characteristic earthquakes: examples from the Wasatch and San Andreas faults. Journal of Geophysical Research 89, 5681–5698.

Schwartz, D.P,, Coppersmith, K.J., 1986. Seismic hazards: new trends in analysis using geologic data. In: Wallace, R.E., (Ed.), Active Tectonics, National Academy Press, pp. 215–230.

Segall, P., Pollard, D.D., 1980. Mechanics of discontinuous faults. Journal of Geophysical Research 85, 4337–4350.

Sibson, R.H., 1985. Stopping of earthquake ruptures at dilatational jogs. Nature 316, 248–251.

Sotiriadis, L., Psilovikos, A., Astaras, Th., 1972. Origin and formation of some characteristic geomorphological occurrences in the tectonic valley of Langada-Volvi, "Nymphopetres". Scientific Annales Faculty of Sciences, Aristotle University of Thessaloniky 12, 59–65.

Soufleris, C., Stewart, G.S., 1981. A source study of the Thessaloniki (Northern Greece) 1978 earthquake sequence. Geophysical Journal of the Royal Astronomical Society 67, 343–358.

Soufleris, C., Jackson, J.A., King, G.C.P., Spencer, C., Scholz, C., 1982. The 1978 earthquake sequence near Thessaloniki (northern Greece). Geophysical Journal of the Royal Astronomical Society 68, 429–458.

Syrides, G., 1990. Lithostratigraphic, biostratigraphic and paleostratigraphic study of the Neogene–Quaternary sedimentary formations of Chalkidiki peninsula. Ph.D. Thesis, University of Thessaloniki, in Greek.

Tranos, M.D., 1998. Contribution to the study of the neotectonic deformation in the region of Central Macedonia and North Aegean. Ph.D. Thesis, University of Thessaloniki, in Greek.

Tranos, M.D., Mountrakis, D.M., 1998. Neotectonic joints of northern Greece; their significance on the understanding of the active deformation. Bulletin of Geological Society of Greece 32, 209–219.

Tranos, M.D., Pavlides, S.B., Mountrakis, D.M., 1995. Neotectonic joints, indicators of the contemporary stress directions in the seismically active Chalkidiki peninsula (N. Greece). In: Rossmanith, H.P., (Ed.), Mechanics of Jointed and Faulted Rock, Balkema, pp. 267–272.

Tranos, M.D., Kilias, A.A., Mountrakis, D.M., 1999. Geometry and kinematics of the Tertiary post-metamorphic Circum Rhodope Belt Thrust System (CRBTS), Northern Greece. Bulletin of Geological Society of Greece 33, 5–16.

Wessel, P., Smith, W.H.F., 1995. New version of the Generic Mapping Tools released. Eos 76, 329.